

Global Biogeochemical Cycles®



RESEARCH ARTICLE

10.1029/2022GB007578

Coastal N₂ Fixation Rates Coincide Spatially With Nitrogen Loss in the Humboldt Upwelling System off Peru

Leila R. Kittu¹ , Allanah J. Paul¹, Mar Fernández-Méndez^{1,2} , Mark J. Hopwood^{1,3} , and Ulf Riebesell¹ 

¹Marine Biogeochemistry, GEOMAR Helmholtz Centre for Ocean Research Kiel, Kiel, Germany, ²Now at Alfred Wegener Institute Helmholtz Centre for Polar and Marine Research, Bremerhaven, Germany, ³Now at Southern University of Science and Technology, Shenzhen, China

Key Points:

- A north-to-south pattern in N₂ fixation rates was observed, implying increased N turnover between 12°S and 16°S where N loss was pronounced
- The highest N₂ fixation rates were measured in coastal productive waters above and within the Oxygen Minimum Zone, showing no clear relationship with Fe or P
- The magnitude of N₂ fixation was low compared to predictions, estimated to account for ~0.3% of primary production and <2% of local N loss

Supporting Information:

Supporting Information may be found in the online version of this article.

Correspondence to:

L. R. Kittu,
lkittu@geomar.de

Citation:

Kittu, L. R., Paul, A. J., Fernández-Méndez, M., Hopwood, M. J., & Riebesell, U. (2023). Coastal N₂ fixation rates coincide spatially with nitrogen loss in the Humboldt Upwelling System off Peru. *Global Biogeochemical Cycles*, 37, e2022GB007578. <https://doi.org/10.1029/2022GB007578>

Received 5 SEP 2022

Accepted 24 JAN 2023

Author Contributions:

Conceptualization: Leila R. Kittu, Allanah J. Paul, Mar Fernández-Méndez, Mark J. Hopwood, Ulf Riebesell
Formal analysis: Leila R. Kittu
Funding acquisition: Ulf Riebesell
Investigation: Leila R. Kittu, Allanah J. Paul, Mar Fernández-Méndez
Writing – original draft: Leila R. Kittu
Writing – review & editing: Leila R. Kittu, Allanah J. Paul, Mar Fernández-Méndez, Mark J. Hopwood, Ulf Riebesell

© 2023. The Authors.

This is an open access article under the terms of the [Creative Commons Attribution License](https://creativecommons.org/licenses/by/4.0/), which permits use, distribution and reproduction in any medium, provided the original work is properly cited.

Abstract Marine nitrogen (N₂) fixation supports significant primary productivity in the global ocean. However, in one of the most productive regions of the world ocean, the northern Humboldt Upwelling System (HUS), the magnitude and spatial distribution of this process remain poorly characterized. This study presents a spatially resolved data set of N₂ fixation rates across six coastal transects of the northern HUS off Peru (8°S–16°S) during austral summer. N₂ fixation rates were detected throughout the waters column including within the Oxygen Minimum Zone (OMZ) between 12°S and 16°S. N₂ fixation rates were highest where the subsurface OMZ (O₂ < 20 μmol L⁻¹) was most intense and estimated nitrogen (N) loss was highest. There, rates were measured throughout the water column. Hence, the vertical and spatial distribution of rates indicates a collocation of N₂ fixation with N loss in the coastal productive waters of the northern HUS. Despite high phosphate and total dissolvable iron (TdFe) concentrations throughout the study area, N₂ fixation was still generally low (1.19 ± 3.81 nmol L⁻¹ d⁻¹) and its distribution could not be directly explained by these two factors. Our results suggest that the distribution was likely influenced by a complex interplay of environmental factors including phytoplankton biomass and organic matter availability, and potentially iron, or other trace metal (co)-limitation of both N₂ fixation and primary production. In general, our results support previous conclusions that N₂ fixation in the northern HUS plays a minor role as a source of new N and to replenish the regional N loss.

Plain Language Summary High phytoplankton productivity in the Humboldt Upwelling System (HUS) is underpinned by a rich supply of nutrients, such as nitrate, brought to shelf surface waters from depth. However, marine microbes use up some of the nitrate in low-oxygen waters, converting it back to nitrogen gas (N₂). Future climate change projections indicate that nitrate availability may decline in the surface ocean. Less phytoplankton growth in the HUS due to reduced nitrate supply could impact ocean services such as fish production and biological carbon drawdown. Previous studies hypothesize that biological nitrogen fixation by microbes could supply nitrogen and is present in the HUS. Here, we studied the distribution and amount of nitrogen fixation in this region in relation to environmental conditions to better understand if the inputs and losses of nitrogen are balanced. Our results indicate that nitrogen fixation rates are too low to counterbalance the local nitrogen loss and do not contribute significantly to the nitrogen supply for phytoplankton growth. The availability of phosphate and iron is thought to control biological N₂ fixation rates on a global scale, but within the HUS, we are unable to find evidence for this suggesting that other environmental factors, such as organic matter availability, control biological nitrogen fixation.

1. Introduction

Bioavailable nitrogen such as nitrate, nitrite, or ammonium limits marine primary productivity in surface waters due to fast phytoplankton uptake relative to the supply (Moore et al., 2013). Therefore, processes that supply nitrogen (N) to the surface ocean are key to regulating marine productivity and the associated export of carbon to the deep ocean (Gruber, 2004). In the marine environment, the uptake of dinitrogen gas (N₂) by nitrogen-fixing microbes (diazotrophs) is widely recognized as a significant source of new bioavailable N (Gruber & Galloway, 2008). Therefore, diazotrophy has the potential to regulate marine productivity and influence the strength of the biological carbon pump (Karl et al., 2012). An understanding of the spatial distribution of N₂ fixation and the factors that regulate the growth of diazotrophs is therefore essential to comprehending past and future changes in bioavailable N and the associated ecosystem services.

At a steady state, and at a global scale, inputs of bioavailable N to the oceans should be at equilibrium with the loss of N through microbially mediated processes such as denitrification and anammox (anaerobic ammonium oxidation). To keep the global marine N inventory at equilibrium, stabilizing feedback mechanisms between N gain and N loss processes are thereby required. Inputs of bioavailable N are thought to be spatially separated from losses due to factors such as iron (Fe) limitation, temperature, and macronutrient availability, which constrain diazotrophy and influence diazotrophs' response to the local N loss (Gruber, 2004). Whilst N_2 fixation is primarily known to take place in surface waters of open ocean environments, about a third of the global ocean N loss is ascribed to Oxygen Minimum Zones (OMZs, Karstensen et al., 2008). In these zones, oxygen (O_2) concentrations are low enough for both N loss mechanisms, denitrification, and anammox to take place (OMZ is loosely defined herein as $O_2 < 20 \mu\text{mol L}^{-1}$, Text S1 in Supporting Information S2) (DeVries et al., 2012). The OMZ in the Eastern Tropical South Pacific (ETSP) is one such region where a substantial portion of global N loss is known to occur (Hamersley et al., 2007; Kalvelage et al., 2013). As a result of the low O_2 concentrations in subsurface waters of the ETSP, preferential N loss over phosphate (P) results in surplus P conditions over available nitrate in the water column (P^* , defined using the Redfield N:P ratio of 16, Deutsch et al., 2007; Redfield, 1958). In addition, and of direct relevance to diazotrophs given the high Fe requirement of the N_2 fixing enzyme nitrogenase, there is a pronounced release of Fe from shelf sediments into the water column (Kustka et al., 2003; Noffke et al., 2012). These conditions of increased phosphate relative to N, and high iron availability should theoretically favor the growth of diazotrophs. As a result, biogeochemical models have predicted that high N_2 fixation in the ETSP could potentially replenish the intense N loss taking place in subsurface coastal waters (Deutsch et al., 2007). However, contrasting observational and biogeochemical evidence for spatial separation of N_2 fixation and N loss suggests that the regional N inventory in the ETSP could be balanced by external N inputs through high N_2 fixation rates observed in the Western Tropical South Pacific (Bonnet et al., 2017; Wang et al., 2019). Therefore there is uncertainty concerning the role of N_2 fixation in the ETSP and to what extent it may balance the regional N loss.

A biogeochemical model by Landolfi et al. (2013) demonstrated that the collocation of N_2 fixation and N loss, as hypothesized for the ETSP OMZ (Deutsch et al., 2007), could result in a self-sustaining destabilizing feedback in the N cycle. This emanates from a theoretical stoichiometric imbalance, whereby the denitrification of newly fixed organic matter occurs at a higher inorganic N:P ratio (120:1) than N_2 fixation inputs under Redfield conditions (N:P \sim 16:1, Paulmier et al., 2009). This results in an enhanced N deficit, which could stimulate more N_2 fixation. A vicious cycle can ensue if this feedback persists, whereby complete remineralization of organic matter associated with newly fixed N via N_2 fixation would lead to a net loss of bioavailable N from the system. To date, this hypothesized feedback and its implications on the local and global marine N inventory have yet to be assessed. Due to a scarcity of data, and a limited geographical range of observations, N_2 fixation estimates from regions with intensive N loss are mainly based on a few measurements extrapolated to large regions. Given the high spatial and temporal variability of diazotrophic abundances, activities, and species distributions (Gradoville et al., 2017), especially across dynamic shelf regions, these extrapolations have considerable uncertainties. For the ETSP in particular, it is still unclear, for example, how temporal patterns of N_2 fixation may be influenced by long-term climate variability and environmental changes associated with the El Niño–Southern Oscillation dynamics, to which N loss processes such as denitrification have been shown to respond sensitively to (Yang et al., 2017).

Furthermore, there is an ongoing debate concerning the extent to which N_2 fixation rates are controlled by environmental conditions such as in situ O_2 , temperature, organic matter, phosphate, and iron availabilities (Knapp et al., 2016; Luo et al., 2014; Wang et al., 2019). Currently, there is only limited evidence to support a clear link between excess phosphate and Fe availability as primary regulators of N_2 fixation rates within the OMZ of the ETSP (Bonnet et al., 2013; Chang et al., 2019; Dekaezemacker et al., 2013; Fernandez et al., 2015; Löscher et al., 2014; Selden et al., 2021; Wang et al., 2019), despite these factors being widely attributed to determining the spatial niche in which diazotrophy can occur (Ward et al., 2013). However, a confounding factor in assessing the role, particularly of Fe, on diazotrophy is that trace metal concentrations are rarely measured in parallel with N_2 fixation rates, partly due to high chances of sample contamination. This could be a contributing factor to the apparent lack of a clear relationship between Fe and measured N_2 fixation rates. To investigate the distribution and magnitude of N_2 fixation in relation to environmental conditions in the ETSP, we conducted measurements across 6 transects from north to south of the northern HUS off the Peruvian coast. We measured N_2 fixation across gradients of latitude, and physical and biogeochemical conditions, including Fe concentrations within the incubations, used to determine N_2 fixation rates. We aimed to evaluate the distribution of N_2 fixation in

relation to environmental conditions and assess the potential collocation of N_2 fixation and estimates of bioavailable N loss in the northern HUS.

2. Materials and Methods

2.1. Study Area and Hydrographic Sampling

The cruise took place during a warm austral summer (23 December 2018, to 30 January 2019) characterized by ~ 0.7 – 0.8°C above average sea surface temperatures (SSTs) and weak southeast trade winds during an El Niño. We measured N_2 fixation rates, nutrient concentrations, and hydrographic data from 26 stations in the ETSP onboard RV Maria S Merian (cruise MSM 80). Sampling extended along six transects (Figure 1) off Peru from $8^\circ 30'S$ to $16^\circ 30'S$ at distances of 4–293 km from the shore. Our sampling strategy was optimized to cover spatial and vertical water column gradients of O_2 , micronutrients and macronutrients, primary productivity, and light and upwelling intensities.

At each station, vertical depth profiles of temperature, salinity, dissolved oxygen (O_2), photosynthetically-active radiation (PAR), chlorophyll *a* fluorescence, and turbidity were obtained using a Seabird (SBE-911 plus, Seabird-Electronics, USA) conductivity-temperature-depth (CTD) profiler equipped with double temperature (SBE 3) and O_2 sensors (SBE43), a LI-COR Bio spherical PAR sensor and a Wet Labs ECO-FLNTURTD chlorophyll-turbidity sensor. O_2 concentrations from discrete water samples (Winkler titration) were used to calibrate the CTD oxygen sensor. The CTD and sensors were mounted on a 21×10 L Niskin bottle rosette water sampler from which discrete water samples were collected.

Satellite-derived MODIS Chl *a* (NASA Ocean Biology Processing Group, 2017) and SSTs (NASA/JPL, 2020) were downloaded as 8-day composites covering the dates each transect was sampled: Transect 1 (27–31 December 2018), Transect 2 and 3 (1–8 January 2019), Transect 4 and 5 (9–16 January 2019) and Transect 6 (17–24 January 2019).

2.2. N_2 Fixation Incubations and Particulate Matter Isotopic Composition

Seawater samples from each station were collected from four to six depths distributed from the surface (~ 5 – 10 m) to a maximum of 300 m covering the OMZ ($O_2 < 20 \mu\text{mol L}^{-1}$). A subsample (0.4–1.5 L) was immediately filtered (GF75, Advantec, 25 mm \varnothing , 0.3 μm nominal pore size) for the natural abundance of Particulate Organic Carbon (POC) and nitrogen concentrations (PON) and isotopic compositions ($\delta^{13}\text{C}_{\text{POC}}/\delta^{15}\text{N}_{\text{PON}}$).

N_2 fixation rates were determined from triplicate incubations following the modified ^{15}N - N_2 dissolution technique (Großkopf et al., 2012; Mohr et al., 2010). 2.3 L Nalgene transparent polycarbonate bottles were precleaned with 10% HCL and rinsed three times to minimize trace metal contamination before filling with seawater samples. Oxygen contamination during seawater collection was minimized by filling the bottles gently and bubble-free from the bottom with a tube, allowing the overflow of about half the bottle volume before closing the bottle headspace free with septa-fitted caps. The same method was applied for collecting Winkler samples that were used for CTD calibration. Incubation bottles were amended with 100 mL of ^{15}N - N_2 -enriched seawater (Text S2 in Supporting Information S2) yielding an average dissolved N_2 isotope abundance (^{15}N atom %) of 3.90 ± 0.02 atom % (mean \pm SD) in the incubation bottle. Blank incubations using atmospheric air instead of ^{15}N - N_2 isotope addition were performed to track any natural changes in the $\delta^{15}\text{N}$ that may not have been a result of ^{15}N - N_2 addition. The use of air for the blank incubation introduced negligible amounts of dissolved O_2 changes against background concentrations calculated to range between 0%–0.6% in OMZ incubations and 0%–0.14% in euphotic zone incubations. Bottles were incubated for 24 hr in on-deck incubators with a continuous flow of surface seawater. Incubators were shaded to receive 100, 40%, 30%, 15%, 5%, and 0% (Lagoon blue neutral density light screens, Lee light filters) of incoming PAR corresponding to approximate in situ PAR conditions of sampled depths. After 24 hr, entire incubation bottles or, in cases of high biomass, subsamples from individual incubations (range of PON on filter 4.73–177.02 $\mu\text{g}/\text{filter}$) were filtered under gentle pressure (200 mbar) onto precombusted GF75 (Advantec, 25 mm \varnothing , 0.3 μm nominal pore size) and treated with acid (1M HCL for 2 min) to remove particulate inorganic carbon. Filters were oven-dried overnight at 60°C , packed in tin capsules and pelleted for further analysis. All filters were analyzed for POC/N concentration and isotopic composition ($\delta^{13}\text{C}_{\text{POC}}/\delta^{15}\text{N}_{\text{PON}}$) on an

elemental analyzer (Flash EA, ThermoFisher) connected to a mass spectrometer (Delta V Advantage Isotope Ratio MS, ThermoFisher) with the ConFlo IV interface (ThermoFisher).

2.3. N₂ Fixation Rates, Limits of Detection, and Error Analysis

Volumetric absolute N₂ fixation rates were computed as shown in Equation 1 according to Montoya et al. (1996).

$$\text{N}_2 \text{ fixation rate} = \frac{A_{\text{PON}}^{t=f} - A_{\text{PON}}^{t=i}}{A_{\text{N}_2} - A_{\text{PON}}^{t=i}} \times \frac{[\text{PON}]}{\Delta t} \quad (1)$$

Whereby A_{PON} represents the isotope abundance (¹⁵N atom %) of PON in the natural abundance samples ($t = 0$), blank ($t_f = i$) and final ($t = f$) incubations respectively. A_{N_2} represents the isotope abundance of the dissolved inorganic N₂ pool (added + ambient) available to N₂ fixers calculated according to White et al. (2020), and Δt represents the incubation period. The concentration of added ¹⁵N₂ gas in the enriched water was estimated from ideal gas law and the ambient N₂ gas was estimated using gas solubility equations adapted from Weiss (1970) (Text S2 in Supporting Information S2). Following a Wilcoxon test for paired samples between the blank incubation and the natural abundance, we observed a significant difference in the isotope abundance of the PON between the two sets of samples (Figure S1 in Supporting Information S1), indicating that natural changes were taking place in the incubations, independent of isotope addition. Hence, we used the ¹⁵N atom% enrichment from the blank incubation rather than the natural abundance for our calculation to ensure that detectable changes in the $\delta^{15}\text{N}$ isotope signal from our amended incubations account for naturally occurring changes and bottle effects that were not associated with ¹⁵N₂ tracer addition.

For each station, volumetric rates were trapezoidal depth-integrated (areal rates) from the surface through to the maximum depth sampled per station (depth range = 20–250 m). To integrate rates, we assumed that N₂ fixation rates were constant from the surface (0 m) to the depth of the shallowest rate (often 5–10 m and always within the surface mixed layer depth). POC concentrations were also integrated to similar depths as N₂ fixation rates.

Limits of detection (LOD) were calculated as described by White et al. (2020) using standard propagation of errors based on observed variability between triplicate samples (Bevington & Robinson, 2002; Gradoville et al., 2017). Any measured N₂ fixation rates below the limit of detection for each respective measurements were assumed to be equal to 0 nmol N L⁻¹ d⁻¹ before any further statistical analysis was performed. See Text S3 in Supporting Information S2 for detailed explanations concerning LOD calculations.

2.4. Inorganic Nutrients, Chl *a*, and Trace Metal Analyses

Unfiltered samples for dissolved inorganic nitrogen (nitrate (NO₃⁻), nitrite (NO₂⁻) and ammonium (NH₄⁺), hereafter DIN), phosphate (PO₄³⁻ or DIP), and silicate (Si(OH)₄) were collected in triplicate. Concentrations were measured onboard using an autosampler (XY-2 autosampler, SEAL Analytical) and a continuous flow analyzer (QUAAtro Autoanalyzer, SEAL Analytical) according to Holmes et al., 2011; Morris & Riley, 1963; Murphy & Riley, 1962. The LOD was calculated from blank measurements as blank +3 times the standard deviation of the blank during each measurement (LOD NO₃⁻ = 0.133 μmol L⁻¹, NO₂⁻ = 0.011 μmol L⁻¹, NH₄⁺ = 0.040 μmol L⁻¹, Si(OH)₄ = 0.130 μmol L⁻¹, PO₄³⁻ = 0.009 μmol L⁻¹). The precision of the measurements was estimated from the average standard deviation between triplicate measurements (NO₃⁻ = 0.028 μmol L⁻¹, NO₂⁻ = 0.018 μmol L⁻¹, NH₄⁺ = 0.029 μmol L⁻¹, Si(OH)₄ = 0.013 μmol L⁻¹, PO₄³⁻ = 0.003 μmol L⁻¹). Dissolved organic phosphorus (DOP) was measured using the persulfate oxidation approach outlined in Hansen & Koroleff, 1999 with an oxidizing decomposition reagent (Merck, Germany). P* was calculated from DIN (NO₃⁻ + NO₂⁻ + NH₄⁺) and DIP measurements after Deutsch et al. (2007) using Equation 2 where R_{16:1} is the integrated ratio of DIN and DIP in seawater and organic matter (Redfield, 1958).

$$\text{P}^* = [\text{PO}_4^{3-}] - \frac{[\text{NO}_3^-] + [\text{NH}_4^+] + [\text{NO}_2^-]}{\text{R}_{16:1}} \quad (2)$$

To measure total dissolvable (Td) trace metal concentrations available within our N₂ fixation incubations, seawater samples were taken unfiltered from the Niskin bottle where N₂ fixation samples were collected. Samples were retained in 125 ml low-density polyethylene sample bottles (Nalgene) which had been precleaned

with Mucosal®, followed by 1 week in 3 M HCl and 1 week in 3 M HNO₃ with 3 deionized water rinses after each stage. Plasticware for sampling was cleaned similarly. Sample bottles were prerinsed three times with a few milliliters of the sample before filling. Sample bottles were stored double-sealed in pre-cleaned sample bags. Total dissolved trace metal concentrations were determined via inductively coupled plasma mass spectrometry (ICPMS) after preconcentration as per Rapp et al. (2017). Samples were acidified with ultrapure hydrochloric acid (UpA grade, Romil) to pH 1.9 and left sitting for >6 months, subjected to 4 hr UV irradiation in 30 mL fluorinated ethylene propylene bottles, preconcentrated offline using a SeaFAST system (Elemental Scientific Inc), and then analyzed on an Element XR ICPMS (Thermo Finnigan). The trace metal reference material CASS-6 was also analyzed to assess the accuracy of the analytical procedure (Table S1 in Supporting Information S1).

As the main purpose of measuring total dissolvable iron (TdFe) was to ascertain the Fe available to diazotrophs at incubation, which may diverge from ambient concentrations, some degree of contamination would not detract from the purpose of the study. At 3 stations, which were 6, 9, and 234 km from the coast, triplicate samples were taken to check for data reproducibility (Figure S2a in Supporting Information S1). The similarity of triplicate TdFe samples (Figure S2a in Supporting Information S1) suggests a limited degree of random contamination, and concentrations are in the range of Total particulate Fe and dissolved Fe concentrations determined on a prior cruise (Hopwood et al., 2021) with a GEOTRACES compliant trace metal clean rosette system and clean lab (Figure S2b in Supporting Information S1). Due to a dominant benthic Fe source in this region, the extremely high TdFe concentrations are realistic for coastal shallow stations (Chever et al., 2015) and would likely mask any modest degree of Fe contamination during handling (Figure S2b in Supporting Information S1).

To assess trace metal and macronutrient coupling, we calculated a diagnostic tracer as a measure of Fe colimitation with PO₄³⁻ (TdFe_p^{*}) using Equation 3 (Parekh et al., 2005; Tang, Wang et al., 2019). R_{Fe:P} represents average phytoplankton uptake requirements for multiple nutrient availabilities based on the extended Redfield ratio (C_{7.75}N₁Si₁P_{0.0626})₁₀₀₀Fe_{0.469} (Moore, 2016). Positive values for TdFe_p^{*} suggest that Fe is in excess relative to measured PO₄³⁻, while negative values indicate Fe deficiency.

$$\text{TdFe}_p^* = [\text{TdFe}] - R_{\text{Fe:P}} \times [\text{PO}_4^{3-}] \quad (3)$$

2.5. Estimating Fixed Nitrogen Loss

In order to estimate water column N loss, a DIN deficit (N_{def}) method, as described originally by Codispoti et al. (2001), was used. N_{def} estimates the amount of fixed nitrogen removed from a parcel of water integrated over space and time assuming no mixing. N_{def} was estimated as the difference between the expected DIN (N_{exp}) considering that N loss was absent and the observed DIN (N_{obs}) from our study according to Equation 4 by Chang et al. (2010). N_{exp} was calculated considering Redfield (Redfield, 1958) organic matter respiration regenerating a local average inorganic N:P ratio of 15.8 for waters outside the ETSP OMZ where anaerobic DIN loss is assumed to be 0. The value 0.3 μmol L⁻¹ denotes the concentration of PO₄³⁻ remaining when DIN is zero in the N:P relationship. Based on this definition, positive values of N_{def} estimate DIN loss that has occurred in a water mass within the Peruvian OMZ.

$$N_{\text{def}} = 15.8 [\text{PO}_4^{3-} - 0.3] - [\text{NO}_3^- + \text{NH}_4^+ + \text{NO}_2^-] \quad (4)$$

2.6. Statistical Analyses

Across the entire data set of N₂ fixation, a Spearman's rank correlation was used to examine the potential relationships between N₂ fixation rates and physical, biogeochemical, and biological parameters across the northern HUS.

Gradients in biogeochemical variables could influence the magnitude and distribution of N₂ fixation rates in the water column. Therefore, three water column depth horizons were identified based on PAR/fluorescence and O₂ concentrations: the euphotic zone (oxic waters within the euphotic zone), the oxic zone (describing all sampled depths below the euphotic zone with O₂ concentrations >20 μmol L⁻¹) and the OMZ zone (describing deeper

depths where O_2 concentrations were $<20 \mu\text{mol L}^{-1}$). See Text S1 in Supporting Information S2 for further details of how depth horizons were delimited. Measurements of N_2 fixation rates, and physical and biogeochemical variables were then grouped based on the depth horizons. To test for the differences in the distribution of N_2 fixation rates and physical and biogeochemical variables between the three depth horizons, a nonparametric one-way analysis of variance (ANOVA) with the Kruskal-Wallis test was performed. A Dunns multiple comparison test was applied post hoc to analyze differences between every pair of groups. By applying these two techniques, we increased the chance to reveal relationships that may not follow a linear distribution.

The spatial distribution of some environmental variables such as measured O_2 , satellite-derived SSTs, and surface Chl *a* from MODIS were interpolated using the Akima package in R (Hiroshi Akima [aut, cph] (Fortran code (TOMS 760, 761, 697 and 433)) et al., 2021). All statistical analysis and data visualizations were performed using R studio version 1.3.959.

3. Results

3.1. Oceanographic Conditions

Our cruise took place in the northern HUS, covering almost half of the Peruvian coast from north to south (Figure 1a). Our stations encompassed coastal locations where the lower boundary of the OMZ is ~ 600 m, and offshore locations where the lower boundary of the OMZ is >600 m (Kalvelage et al., 2013). Transects 1 and 2 were located on a wide shelf area off northern Peru where mean MODIS SSTs ranged from 21°C to 24°C (Figure 1a) with averages of $22.12 \pm 1.82^\circ\text{C}$ (Table S2 in Supporting Information S1). The vertical temperature and salinity distribution at the time of sampling exhibited a typical upwelling pattern of low surface temperatures ($\sim 20^\circ\text{C}$) and a reduced vertical temperature gradient close to shore with low salinity waters (<35.1 , Figures S3, and S4 in Supporting Information S1). A pronounced subsurface salinity maximum developed past the shelf edge, probably as a result of offshore drift of high salinity waters. In addition, a thick (~ 70 m depth), well-oxygenated water layer was observed in all stations from the northern transects (Figure 2). The upper boundary of the OMZ ($O_2 = 20 \mu\text{mol L}^{-1}$) extended from 51 to 150 m and O_2 concentrations were below the detection limit ($2\text{--}3 \mu\text{mol L}^{-1}$) in deeper waters between 200 and 650 m depth. In all stations above the shelf from Transects 1 and 2, O_2 concentrations were consistently $>50 \mu\text{mol L}^{-1}$ and an upward shoaling of oxyclines was also observed in stations above the shelf edge, indicating the influence of enhanced mixing and advection in coastal subsurface waters.

Transect 3 covered the central shelf at 12°S off Callao, marking a transition between the north and south of the HUS. Cool mean MODIS SSTs ($\sim 19^\circ\text{C}$) at the coast and salinity gradients indicated active or recent upwelling (Figure 1a). Surface waters were associated with elevated mean MODIS Chl *a* (Figure 1b) and increased turbidity (Table S3 in Supporting Information S1, Figure S6 in Supporting Information S1). In contrast to the northern shelf transects, salinity was in general slightly lower and homogenous throughout the water column (35.05) showing a weak subsurface salinity maximum (Figure S4 in Supporting Information S1). Toward oceanic waters at the transect edge, SSTs slightly increased to 24°C . All stations sampled from Transect 3 were coastal with an OMZ thickness ranging between 80 and 420 m (Figure 2). A shallow OMZ was observed where the upper boundary of the OMZ ranged between 20 and 70 m and O_2 concentrations were below detection between 100 and 550 m.

On the southern Peruvian coast, where the shelf is relatively narrow, hydrographic features between 14.5°S and 16°S indicated that upwelling was active during our sampling. A signal of low O_2 , nutrient-rich waters appeared at the surface (Figures 2 and 4a). Low SST ($\sim 18^\circ\text{C}$) was observed close to the coast accompanied by upward shoaling of oxyclines very close to the coast at 14.4°S (Figure 2, Table S2, Figure S3 in Supporting Information S1). In offshore stations, mean MODIS SSTs reached a maximum of $\sim 22^\circ\text{C}$ and vertical O_2 and temperature profiles indicated a shallow (~ 20 m thick, Figure S3 in Supporting Information S1) well-oxygenated layer of warm surface water. Absolute temperatures and vertical gradients decreased eastwards toward the coastal stations in all southern transects (Transects 4–6). Around 15°S (Transect 5), local vertical shoaling of isotherms was observed above the shelf. High Chl *a* and POC concentrations (Figure 1) were observed in the surface waters of coastal stations in the southern transects consistent with a narrow surface turbidity layer at 15.3°S (Figure S6 in Supporting Information S1). Additionally, a narrow-oxygenated surface water layer was observed, mostly separated from a shallow OMZ by the 17°C isotherm, although O_2 concentrations were still lower than the northern transects (Table S2 in Supporting Information S1). In the southern part of the study area, the upper boundary of the OMZ ranged from 4 to 58 m. Between 50 and 735 m across all stations from Transects 4–6, O_2 was below detection.

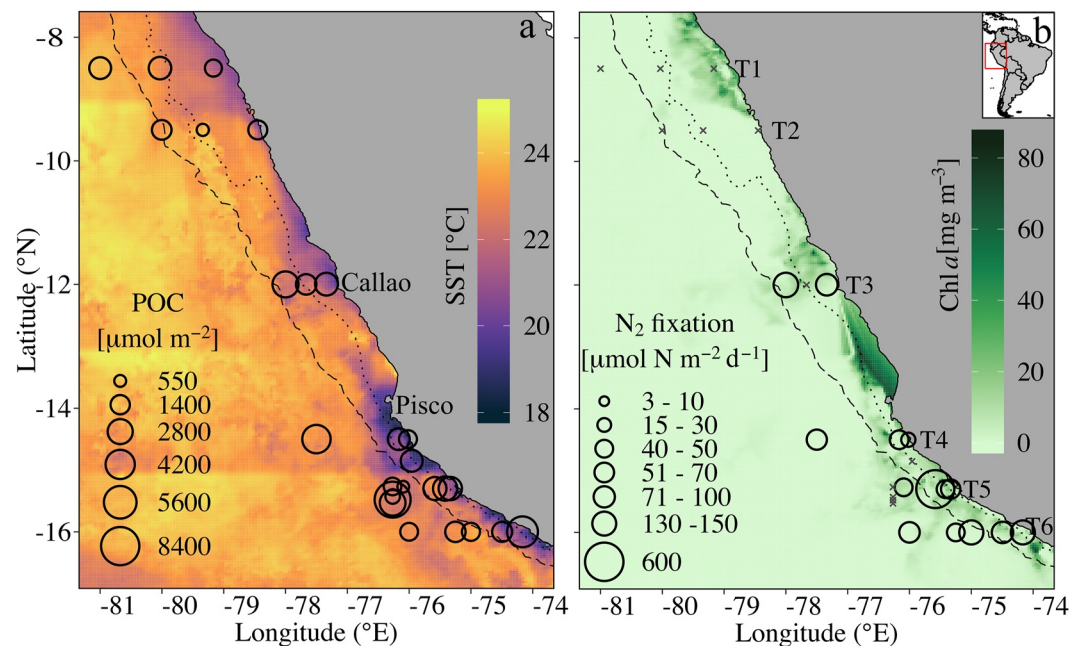


Figure 1. (a) Mean MODIS (NASA/JPL, 2020) sea surface temperature (SST) (SST) in the study area overlain by depth-integrated Particulate Organic Carbon concentrations at each station. (b) Mean MODIS (NASA Ocean Biology Processing Group, 2017) surface Chlorophyll *a* concentration (Chl *a*) overlain by integrated N_2 fixation rates ($\mu\text{mol N m}^{-2} \text{d}^{-1}$) for each station along the six across-shelf transects (T1-T6). Crosses on (b) indicate rates below detection. 8-day average products of SST and Chl *a* covering the dates each transect was sampled were used to generate figures a and b respectively. Black dotted and dashed lines show 200 and 2,000 m bathymetry to indicate the edge of the shelf and shelf slope, respectively.

3.2. N_2 Fixation Rates

Measured N_2 fixation rates showed a latitudinal trend, on average increasing from north to south of the Peruvian coast (Figure 2). This trend was consistent with significant latitudinal differences in SSTs, PO_4^{3-} , P^* , DIN:P , Ndef , turbidity, POC, and PON (Table S2 in Supporting Information S1). Rates ranged between undetectable in the two northern transects (Transect 1 and 2) to a maximum of $30.97 \text{ nmol N L}^{-1} \text{d}^{-1}$ at Transect 5 with an overall average and standard deviation of $1.19 \pm 3.81 \text{ nmol N L}^{-1} \text{d}^{-1}$ ($n = 103$ measurements). Detectable N_2 fixation rates between 12°S and 16°S (Transects 3–6) were measured above the shelf (range $0.38\text{--}30.97 \text{ nmol N L}^{-1} \text{d}^{-1}$ $n = 75$ measurements) corresponding to waters with DIN:DIP ratios below 16 (Figure 3a).

Considering the depth distribution of the rates, the highest mean N_2 fixation rates ($1.73 \pm 4.82 \text{ nmol N L}^{-1} \text{d}^{-1}$, $n = 62$) were measured in warm ($19.3 \pm 2.22^\circ\text{C}$), oxic waters ($>20 \mu\text{mol L}^{-1}$) within the euphotic zone (12–73 m), albeit with high variability between depths (Table S3 in Supporting Information S1). The second highest average rates, $0.45 \pm 0.59 \text{ nmol N L}^{-1} \text{d}^{-1}$ were measured within cooler waters of the OMZ where O_2 concentrations were lowest and P^* and TdFe_p^* were highest (Table S3 in Supporting Information S1) while the lowest average rates were measured from oxic waters ($0.12 \pm 0.40 \text{ nmol N L}^{-1} \text{d}^{-1}$). A Kruskal-Wallis one-way ANOVA testing for the null hypothesis that the distribution of N_2 fixation rates between the depth horizons has identical medians was insignificant (Kruskal-Wallis $p > 0.05$, Table S3 in Supporting Information S1).

N_2 fixation rates were significantly positively correlated with POC, turbidity, and Chl *a*, all factors that were used as proxies for phytoplankton-associated organic matter availability (Figure 3b). In addition, temperature and oxygen were also positively correlated with N_2 fixation. Despite the co-occurrence of high N_2 fixation in surface waters with high DOP concentrations (Table S3 in Supporting Information S1), a weak positive relationship observed between N_2 fixation and DOP was not significant. DIN and DIN:P were both negatively correlated with N_2 fixation rates across the whole data set, with the lowest values observed in southern transects (Transects 4–6, Table S2 in Supporting Information S1).

Depth-integrated N_2 fixation rates (areal, 0–250 m) ranged from 18.20 to $582.11 \mu\text{mol N m}^{-2} \text{d}^{-1}$ (average \pm sd, $124.04 \pm 138.94 \mu\text{mol N m}^{-2} \text{d}^{-1}$), showing latitudinal differences from the central to the southern extent of our

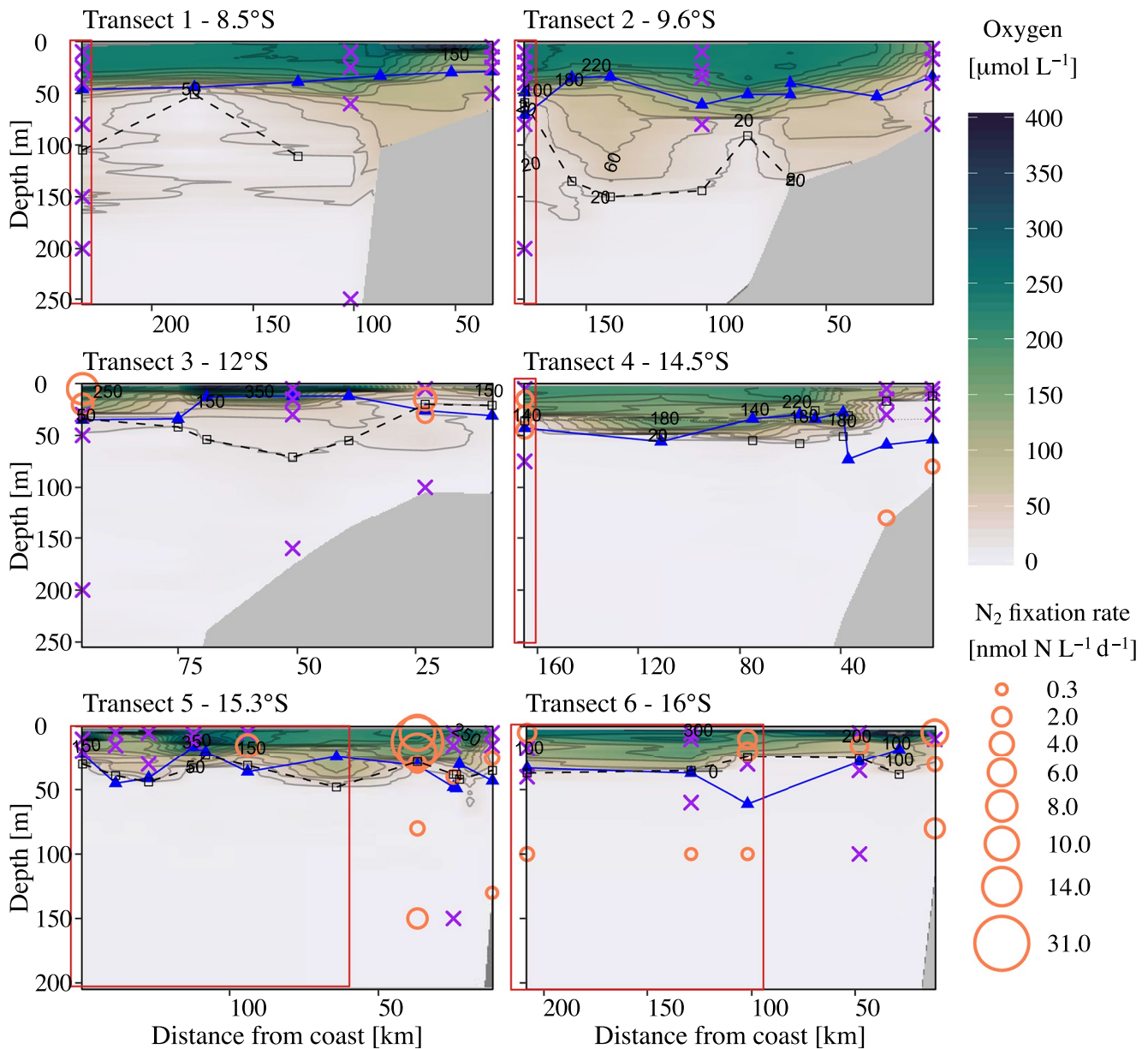


Figure 2. Measured N_2 fixation rates (empty orange circles) overlaid on the vertical distribution of O_2 concentrations ($\mu\text{mol L}^{-1}$) along the six transects. The black dotted lines and blue triangles indicate the upper boundary of the OMZ waters ($O_2 < 20 \mu\text{mol L}^{-1}$) and the depth of the euphotic zone (photosynthetically-active radiation = 1%) respectively. Purple crosses indicate depths where N_2 fixation rates were below detection. The red box indicates offshore stations defined as those in which the lower boundary of the OMZ was >600 m.

study (12°S and 16°S). Albeit with high variability, average areal rates were highest in Transect 5 ($188.15 \pm 262.80 \mu\text{mol N m}^{-2} \text{d}^{-1}$, Figure S5 in Supporting Information S1).

3.3. Macronutrients and Total Dissolved Iron

For all stations, PO_4^{3-} and DIN concentrations in waters above the OMZ ranged between ($0.50\text{--}2.60 \mu\text{mol L}^{-1}$) and ($0.10\text{--}33.17 \mu\text{mol L}^{-1}$) respectively (Figure 4a, Figure S6 in Supporting Information S1). Beyond the respective limits of the euphotic zone across all stations ($12\text{--}73$ m), DIN and PO_4^{3-} concentrations exceeded 15 and $2 \mu\text{mol L}^{-1}$, respectively. DIN:DIP ratios ranged between $0.05\text{--}15.17$ (average in the euphotic zone was 10.00 ± 3.73 , average in oxic waters was 13.76 ± 1.46), indicating a deficit of dissolved inorganic nitrogen throughout the water column (Figure 3, Table S3 in Supporting Information S1). PO_4^{3-} concentrations were low in Transect 1 and 2

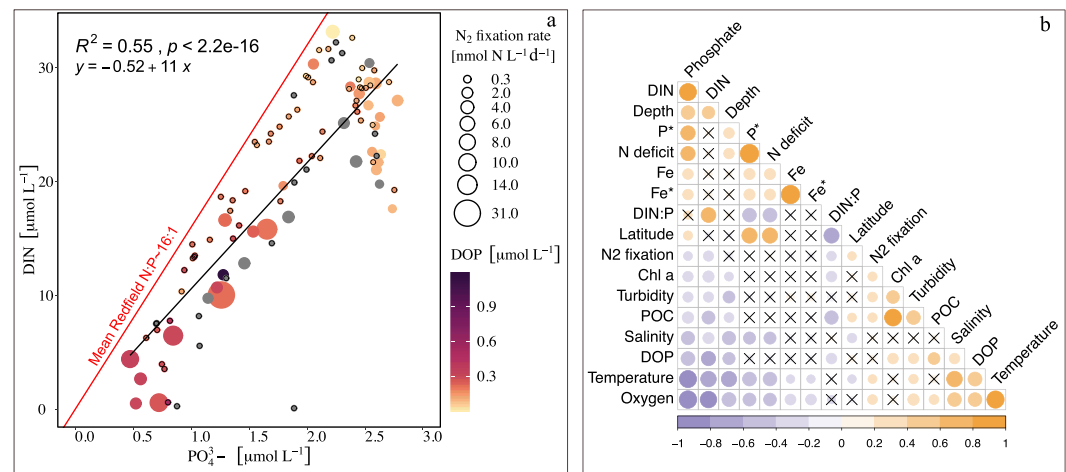


Figure 3. (a) Relationship between DIN and PO_4^{3-} concentrations for all stations during the cruise. The size of the circles corresponds to the measured N_2 fixation rates and the color corresponds to the dissolved organic phosphorus concentrations (Dissolved organic phosphorus (DOP)). Gray points and points with black rings depict samples where DOP concentrations and N_2 fixation rates were below the detection limit, respectively. (b) Spearman correlation coefficients plot including N_2 fixation rates and environmental variables ($n = 103$). Positive and negative correlations are displayed in orange and purple respectively. Color intensity and size of circles are proportional to the correlation coefficients. Non-significant correlations (adjusted p -value > 0.05) are indicated by black crosses.

($1.49 \pm 0.56 \mu\text{mol L}^{-1}$) coinciding with high DIN concentrations which resulted in low P^* values (< 0.5) down to 200 m (Figure 4a, Table S3 in Supporting Information S1). For Transects 3–6, PO_4^{3-} concentrations were on average higher ($1.94 \pm 0.68 \mu\text{mol L}^{-1}$) than in the north (Figure 4a). Coupled with slightly lower NO_3^- concentrations, high P^* values were measured ($0.73 \pm 0.35 \mu\text{mol L}^{-1}$) between the central and southern part of our study reflecting DIN loss in most of the water column (Figure 5b, Figure S8 in Supporting Information S1). Upward shoaling of waters with high P^* was observed in OMZ waters throughout the study area, indicating a tendency of upward advection of denitrified waters with high PO_4^{3-} relative to DIN (Figure S8 in Supporting Information S1). DOP concentrations were higher in the euphotic waters ($0.24 \pm 0.17 \mu\text{mol L}^{-1}$) and lower at depth (range = 0 – $0.15 \mu\text{mol L}^{-1}$). The highest DOP concentrations were measured in the surface waters of Transect 4 ($1.18 \mu\text{mol L}^{-1}$) and at a coastal station of Transect 6 ($0.54 \mu\text{mol L}^{-1}$) (Figure S9 in Supporting Information S1).

Total dissolvable iron (TdFe) concentrations were high in most of the incubations with slight differences in TdFe concentrations between the northern ($28.11 \pm 50.61 \text{ nmol L}^{-1}$), central (82.71 ± 127.17), and southern ($36.31 \pm 40.47 \text{ nmol L}^{-1}$) transects (Table S2 in Supporting Information S1). The highest TdFe concentrations were measured from subsurface waters close to the coast at 12°S ($461.84 \text{ nmol L}^{-1}$). Generally, depth distributions indicated lower concentrations in surface waters close to the coast, which occasionally increased toward deeper waters (Table S3 in Supporting Information S1). However, uniformly high TdFe concentrations were measured in the surface waters of stations closest to the coast at 14°S . Concentrations in the euphotic zone (depth range, 12–73 m) ranged from 1.18 to $216.53 \text{ nmol L}^{-1}$ (mean \pm SD = $22.23 \pm 35.03 \text{ nmol L}^{-1}$). In the oxic waters below the euphotic zone, TdFe concentrations increased with depth from 8.06 to $223.49 \text{ nmol L}^{-1}$ (mean \pm SD = $55.70 \pm 78.06 \text{ nmol L}^{-1}$) but showed high variability due to sporadic high concentrations $> 200 \text{ nmol L}^{-1}$ in subsurface waters at most coastal stations in Transect 2. Within O_2 -deficient waters, average concentrations were slightly higher than those in oxic waters but similarly with high variability ($68.22 \pm 87.13 \text{ nmol L}^{-1}$). TdFe $_{\text{P}^*}$ followed a similar pattern as absolute TdFe concentrations (Figure S10 in Supporting Information S1).

3.4. Estimates of Bioavailable Nitrogen Loss

Accumulation of NO_2^- in OMZ waters is considered a signal of active N loss since it is consumed as a substrate for anammox and is an intermediate product of denitrification (Lam et al., 2009). In this study, we use its presence to estimate N loss occurrence and its spatial association with N_2 fixation. To estimate N loss from a water parcel, we calculated the nitrate deficit (N_{def}), estimating conversion of NO_3^- to N_2 gas. Between the northernmost transect at 8°S and the central transect at 12°S , a weak secondary NO_2^- maximum was observed where NO_2^- concentrations

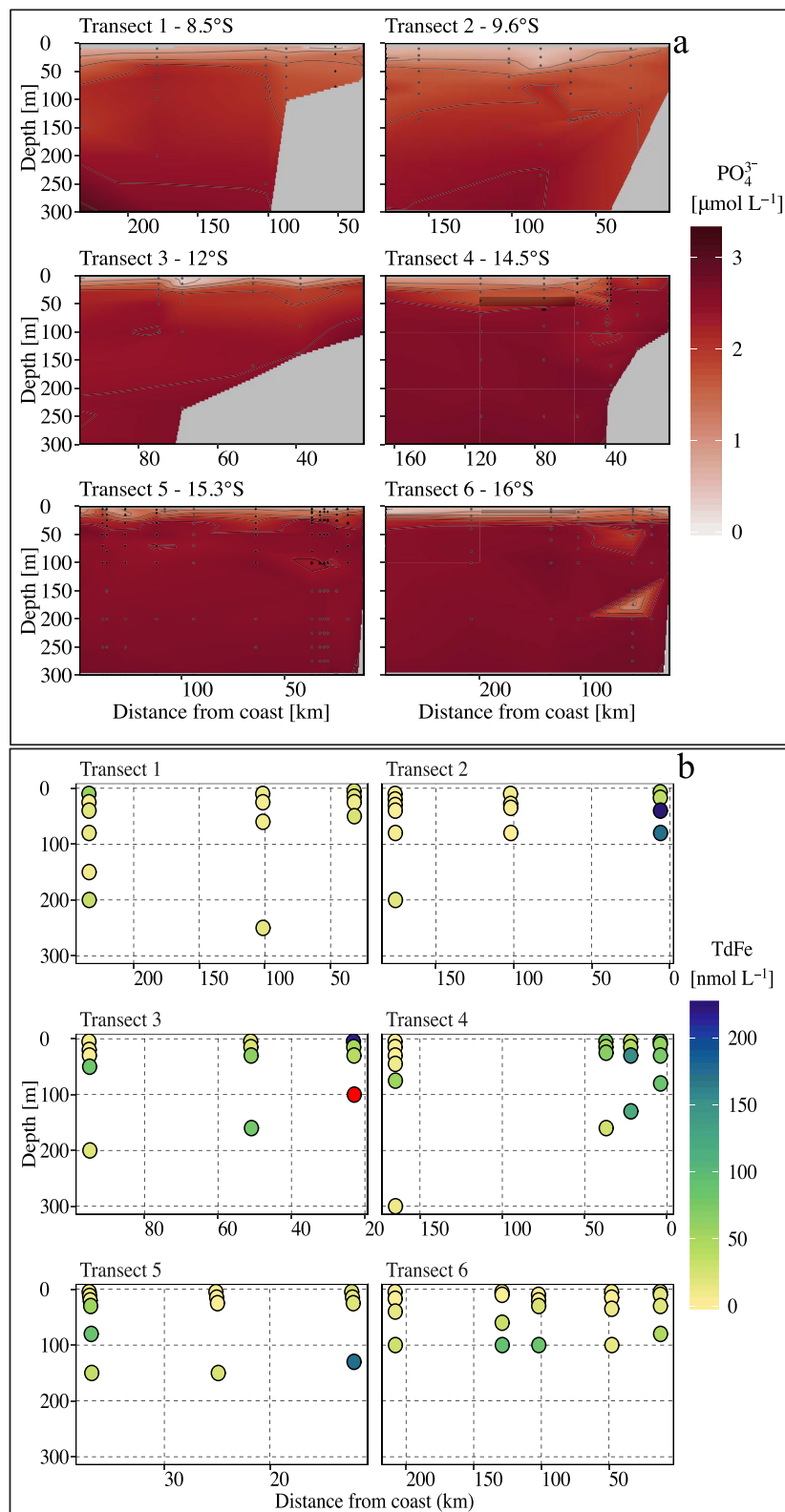


Figure 4. Profiles of (a) PO_4^{3-} concentrations and (b) total dissolvable iron (TdFe) along the 6 transects during the cruise. TdFe data corresponds to measured TdFe in each discrete incubation where N_2 fixation measurements were made. The red dot in figure b indicates the highest TdFe concentration ($461.84 \text{ nmol L}^{-1}$).

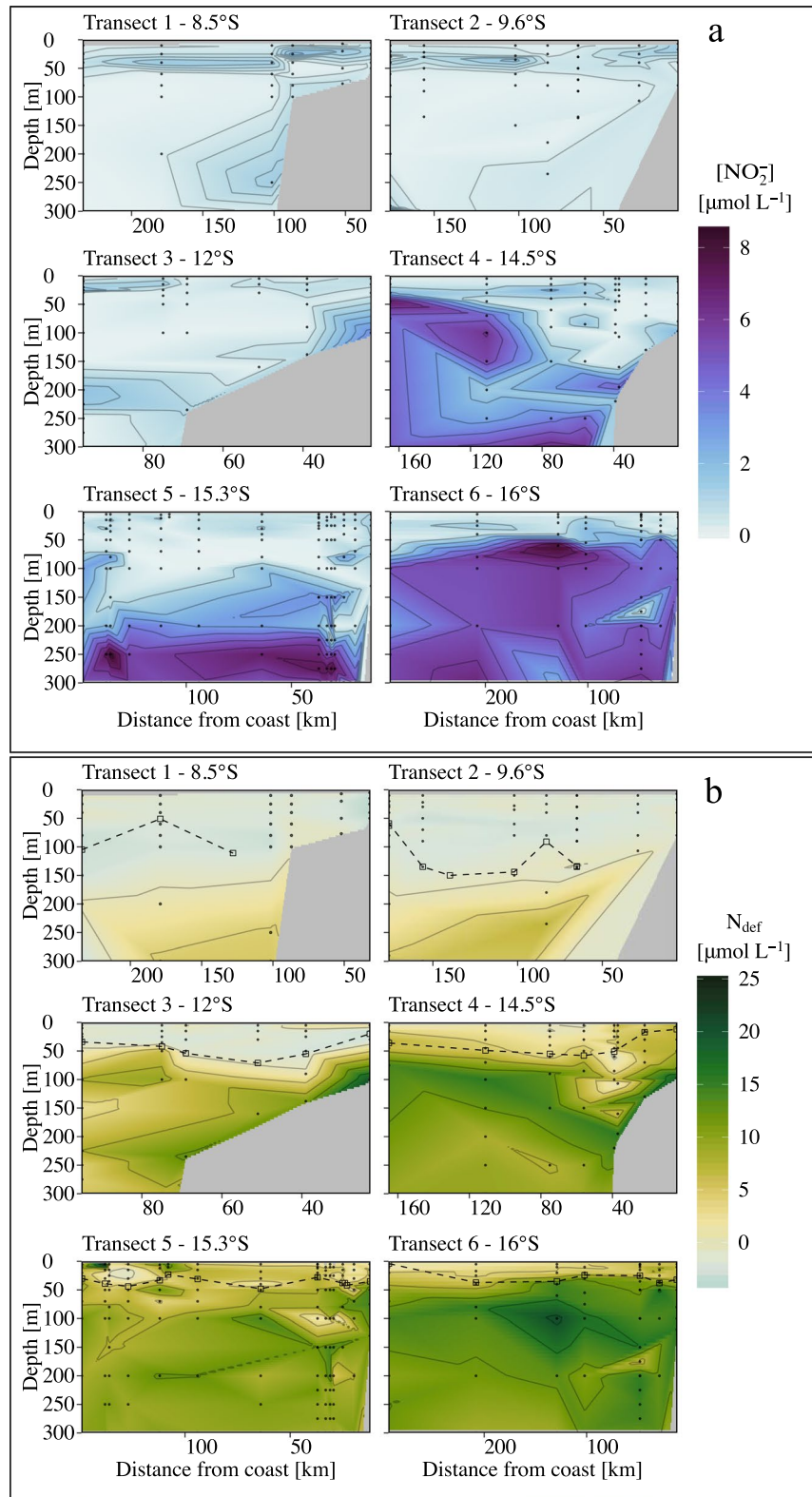


Figure 5. Distribution of (a) nitrite (NO_2^-) concentrations and (b) calculated DIN deficit (N_{def}) along the 6 transects during the cruise. The dotted line in figure b denotes the upper boundary of the OMZ layer with O_2 concentrations $<20 \mu\text{mol L}^{-1}$.

ranged between 0.01–2.14 $\mu\text{mol L}^{-1}$, except for the most coastal station at Transect 3 where subsurface NO_2^- concentrations close to the bottom reached 3.26 $\mu\text{mol L}^{-1}$ (Figure 5a). A weak N_{def} signal (0–5 $\mu\text{mol L}^{-1}$) was observed only in subsurface waters beyond 200 m in Transects 1–3. Above these depths, N_{def} was mostly below 0 $\mu\text{mol L}^{-1}$ (Figure 5b), indicating a reduced active N loss signal in the water mass.

At Transect 4 (14°S), stations closest to the coast had a deeper and pronounced NO_2^- maximum below 150 m. Beyond 50 km distance from the coast, the depth of the secondary NO_2^- maximum from all stations reduced to 50 m. The profile of NO_2^- in Transect 4 indicated a local NO_2^- decline between 100 and 250 m depth (Figure 5a). In Transect 5 where the highest N_2 fixation rates were measured, a much more pronounced secondary NO_2^- maximum was observed in deeper layers, extending from ~100 m, despite a shallow upper boundary of the OMZ from 50 m. Maximum NO_2^- concentrations of up to 8.3 $\mu\text{mol L}^{-1}$ were measured between 250 and 300 m depth at Transect 5. At the most southern transect along 16°S, a sharp oxycline was observed in which NO_2^- was seen to accumulate in shallow OMZ waters from 30 m (Figure 5a) extending to ~300 m and reaching a maximum of 8–8.3 $\mu\text{mol L}^{-1}$ at most stations. Consistent with the occurrence of secondary NO_2^- maxima, our results reveal a strong N loss signal in coastal subsurface waters between 12°S and 16°S, as indicated by positive N_{def} values of up to 25 $\mu\text{mol L}^{-1}$ (Figure 5b, Table S2 in Supporting Information S1). However, this signal was less pronounced in surface waters above the upper boundary of the OMZ (0–<50 m).

4. Discussion

Within the ETSP, previous studies have shown that heterotrophic diazotrophs such as proteobacteria are dominant and contribute significantly to N_2 fixation in the region (Bonnet et al., 2008; Jayakumar & Ward, 2020; Löscher et al., 2014; Turk-Kubo et al., 2014). While unicellular cyanobacterial diazotrophs like *Crocospaera* spp have been observed sporadically, they are not the dominant diazotrophs and their relative contribution to total N_2 fixation in the ETSP is negligible due to substantially low abundances (Bonnet et al., 2008; Löscher et al., 2014; Turk-Kubo et al., 2014). In a previous study by Chang et al. (2019), N_2 fixation rates were detected only in euphotic waters, where the abundances of nitrogenase (*nifH*) copies from proteobacteria were high with a notable lack of sequences from cyanobacterial diazotrophs. This demonstrates that the vertical distribution of heterotrophic diazotrophs in the ETSP is independent of light. Similarly, N_2 fixation rates in our study did not seem to be influenced by light availability as they were measured throughout the water column, from the surface to aphotic waters within the OMZ without significant differences in depth horizons (Table S3 in Supporting Information S1). Based on this evidence, heterotrophic diazotrophy in surface waters cannot be excluded and we argue that the presence of high fixation rates in euphotic waters is not necessarily an indication of autotrophic diazotrophy. Inferring from the aforementioned studies, our observations strongly suggest that the rates we measured here can also be primarily attributed to heterotrophic diazotrophs.

4.1. Spatial and Vertical Distribution of N_2 Fixation Rates in Relation to Environmental Conditions

To the best of our knowledge, this study reports the first extensive distribution of N_2 fixation rates covering a notable part (8°S–16°S) of the coastal northern HUS (4°S–20°S) off the Peruvian coast. It is also one of the few studies to combine N_2 fixation measurements with TdFe concentrations from the incubations. At a global scale, the biogeography of diazotrophy is predicted by considering PO_4^{3-} and Fe availability (Ward et al., 2013), with diazotrophy across most of the ETSP predicted to be limited by low Fe availability (Knapp et al., 2016). Yet on the nearshore spatial scales considered herein, this does not appear to be the case as N_2 fixation rates were often lower than model predictions despite high PO_4^{3-} and TdFe availability.

One noteworthy finding of our study was a latitudinal pattern in the distribution of N_2 fixation rates. All N_2 fixation rates in the north were below detection in comparison to measurable rates in the central and southern latitudes. This could be explained by unfavorable conditions for diazotrophy in the north as conditions controlling N_2 fixation may not be uniform along the coast. Rates below detection in the north were associated with upwelling of highly oxygenated, warm waters (>20°C, Figures 1a and 2, Table S2 in Supporting Information S1). Under such high O_2 conditions, diazotrophs could run into oxidative stress under which the activity of the nitrogenase enzyme is repressed or even inhibited unless O_2 -avoiding mechanisms such as organic particles are utilized (Inomura et al., 2017). However, significantly lower POC concentrations and turbidity in the north (Table S2 in Supporting Information S1) suggest that O_2 -avoiding mechanisms through phytoplankton-associated organic particles

were likely limited in this area. Lack of measurable N_2 fixation rates was also associated with the absence of a secondary NO_2^- maximum ($NO_2^- < 2 \mu\text{mol L}^{-1}$, Figures 2 and 5a), high PO_4^{3-} , TdFe and DIN concentrations (Table S2 in Supporting Information S1). The main Fe source in the Peruvian shelf region is benthic (Chever et al., 2015), and whilst short-term redox dynamics are also clearly important for regulating the inventory of Fe in the water column (Rapp et al., 2020), the highest Fe concentrations are generally expected in the region from ~ 7 to 13°S where the shelf is broad and shallow (Bruland et al., 2005). Hence despite low TdFe concentrations ($< 5 \text{ nmol L}^{-1}$) in some cases, positive $TdFe_p^*$ ($0.27\text{--}222.59 \text{ nmol L}^{-1}$) was observed in all northern stations especially close to the coast indicating that neither phosphorus nor iron limitation seemed to be evident.

Throughout the central and southern part of our study area, detectable N_2 fixation rates between 12°S and 16°S coincided with high surface Chl *a* (Figure 1b), high POC concentrations, high turbidity, higher PO_4^{3-} concentrations and lower O_2 concentrations compared to the northern transects. Correspondingly, a Spearman correlation analysis revealed that across the entire data set, N_2 fixation rates were significantly positively correlated with Chl *a*, POC, and turbidity (Figure 3b). This direct link between N_2 fixation and phytoplankton-associated organic matter has previously been observed in the ETSP and elsewhere in the South West Pacific (Selden et al., 2021; Shiozaki et al., 2014). Organic particles consume O_2 when being remineralized, generating anoxic microniches that can protect heterotrophic N_2 fixation against O_2 inhibition in highly oxygenated waters (Klawonn et al., 2015). This is evident in that dissolved O_2 concentrations were positively correlated with N_2 fixation rates and similarly with POC and turbidity (Figure 3b). Therefore, while O_2 concentrations were still high in surface euphotic waters in the central and southern regions, high particulate organic matter may have increased the presence of anoxic microniches and thereby contributed to mitigating the negative impacts of O_2 availability on N_2 fixation. Organic matter is also a source of energy for heterotrophic N_2 fixation and has been demonstrated to enhance N_2 fixation in experiments in the ETSP (Dekazemacker et al., 2013; Klawonn et al., 2015; Löscher et al., 2014). This would further explain the high N_2 fixation rates in surface productive waters in the southern part of the study area (Figure 1) and the lack of detectable rates in comparatively low productivity and highly oxygenated waters in the two northern transects.

Our measured rates may however be underestimated compared to in situ rates due to incubation artifacts, in particular, elevated incubation compared to in situ temperature as well as potential O_2 contamination. Higher incubation temperatures ($22.91 \pm 1.36^\circ\text{C}$) relative to in situ conditions ($15.21 \pm 1.46^\circ\text{C}$) may have been on the upper end of thermal tolerances for N_2 fixers associated with cool upwelled waters ($3\text{--}18^\circ\text{C}$) such as the Gamma4 γ -proteobacteria abundantly observed from the ETSP (Cheung et al., 2021; Löscher et al., 2014; Turk-Kubo et al., 2014, 2022). Dissolved O_2 concentrations in the incubation bottles may have been higher than in situ because even though we overflowed the bottles with samples to minimize atmospheric contact with the sample, we cannot not completely exclude potential O_2 contamination when filling incubation bottles or during the introduction of isotope-enriched waters. This would result in slightly higher O_2 concentrations in the incubations and potentially higher diffusion of O_2 into organic particles (Chakraborty et al., 2021), which could both act to suppress N_2 fixation rates. While we cannot quantify these effects, this likely had some impact on the profiles of N_2 fixation rates because these factors would make the largest difference in rates where both in situ temperature and O_2 concentrations are lower, such as at depth and in suboxic waters. Nevertheless, these methodological limitations do not compromise the main finding of a latitudinal pattern of N_2 fixation rates but are rather in support of the observed low N_2 fixation rates in northern waters where in situ O_2 and temperature conditions were significantly higher than the south (Table S2 in Supporting Information S1).

Low magnitudes of N_2 fixation rates under phosphate availability is puzzling considering that phosphorus availability has been used to predict high N_2 fixation in this region (Deutsch et al., 2007). A significant negative relationship between N_2 fixation and PO_4^{3-} as indicated by the Spearman correlation analyses could perhaps demonstrate consumption of PO_4^{3-} by the planktonic community, including diazotrophs. However, PO_4^{3-} was not depleted and therefore much higher N_2 fixation rates would be expected for the PO_4^{3-} and TdFe concentrations measured herein if these were the key limiting factors. The residual PO_4^{3-} despite a known important role of phosphorus for diazotrophs may suggest that alternative phosphorus sources or factors may play a primary role in regulating N_2 fixation rates in the study area. Diazotrophs have been shown to synthesize hydrolytic enzymes to acquire P from alternative sources such as DOP (Dyhrman & Haley, 2006; Farnelid & Riemann, 2008; Meyer et al., 2016, 2017; Somes & Oschlies, 2015). However, the low to undetectable DOP concentrations and an insignificant relationship between N_2 fixation and DOP mean our data is insufficient to demonstrate any role of DOP

for N_2 fixation in this study. Nevertheless, evidence that PO_4^{3-} availability did not translate to expected high N_2 fixation suggests the possibility that the diazotroph community in the ETSP may have a different response to PO_4^{3-} availability and/or requirements of alternative phosphorus compounds such as organic phosphorus.

High positive TdFe* throughout the study area (Figure S10, Table S2 and S3 in Supporting Information S1), which is also a common feature of the coastal ETSP (Blain et al., 2008) indicates that there is enough iron, relative to phosphate, to support complete consumption of PO_4^{3-} and thus support N_2 fixation in the coastal waters of the northern HUS. The generally high TdFe availability in this study also indicates the potential for much higher coastal N_2 fixation rates if iron were the major limiting factor for N_2 fixation in the ETSP (Dutkiewicz et al., 2012). Yet higher TdFe concentrations in coastal waters did not always translate to high N_2 fixation rates and in some cases, N_2 fixation rates were not detectable despite TdFe availability (Table S2 in Supporting Information S1). Therefore, the disproportionately low or undetectable N_2 fixation rates despite TdFe availability across most of the incubations from the shelf region is striking. Yet, across the entire data set, slight differences in TdFe concentrations by latitude and coastal-offshore dynamics appeared to be spatially concurrent to differences in N_2 fixation rates (Table S2 and S3 in Supporting Information S1). Despite the high variability in both N_2 fixation rates and TdFe concentrations, general trends indicated that increasing N_2 fixation rates from north to south coincided with a similar increase in TdFe concentrations (Table S2 in Supporting Information S1). Hence, whilst overall TdFe availability suggests that TdFe was nonlimiting and therefore not a major controlling factor for N_2 fixation rates in this study, patterns in the magnitude and distribution of N_2 fixation rates versus the absolute concentrations of TdFe may point towards either further subtleties as to exactly how bioavailable TdFe is to diazotrophs, nonlinearities in its regulation of N_2 fixation, or other chemical, physical and ecological constraints on N_2 fixation. Therefore, dedicated experiments are required to disentangle and understand the complex relationships between Fe availability and N_2 fixation in the ETSP.

From 27 N_2 fixation stations sampled, 11 were characterized as offshore (lower boundary of the OMZ >600 m, Figure 2) and observed to have lower TdFe concentrations (1.18–90.29 $nmol L^{-1}$) relative to coastal stations (1.15–461.84 $nmol L^{-1}$). These differences were associated with higher N_2 fixation rates at most coastal stations than at offshore stations. Our observations are consistent with previous studies reporting the lowest (maximum <1 $nmol N L^{-1} d^{-1}$) to non-detectable rates from open ocean low productivity waters off Peru (Chang et al., 2019; Dekaezemacker et al., 2013; Löscher et al., 2014; Selden et al., 2021). These patterns altogether suggest that while sedimentary iron in coastal waters is high, insufficient iron availability in open ocean waters may to some extent still limit/colimit N_2 fixation in large parts of the ETSP (Wang et al., 2019). Whilst this may occur as a direct influence of TdFe availability on N_2 fixers, it also presents the potential for an indirect effect of iron. Low TdFe availability also limits phytoplankton productivity (Browning et al., 2018; Hutchins et al., 2002), thereby resulting in low organic matter availability, which is attributed to stimulating heterotrophic N_2 fixation (Bombar et al., 2016; Riemann et al., 2022).

Our study highlights that the controlling factors for N_2 fixation may be variable globally among different ocean regions. Specifically for the northern HUS, the controls on N_2 fixation may consist of nonlinear correlations between multiple environmental factors. Therefore, predicting N_2 fixation rates solely on iron and PO_4^{3-} without considering other interlinking factors such as organic matter availability may have resulted in an overestimation of the role and contribution of N_2 fixation in the ETSP (Wang et al., 2019). It is worth mentioning that Chang et al. (2019) did not detect any N_2 fixation activity beyond the euphotic zone during austral winter, additionally revealing the temporal heterogeneity and patchiness of N_2 fixation activity within the northern HUS. Considering the known seasonality and climate-associated variability in physical and biogeochemical conditions such as primary productivity (Messié & Chavez, 2015), which could ultimately influence N_2 fixation in the northern HUS, we hypothesize that seasonal variability of N_2 fixation rates is likely to occur, but will be challenging to constrain due to the sporadic occurrence of high N_2 fixation rates in summer (Fernandez et al., 2011; Löscher et al., 2014), and the time period of observations required to extract seasonal variability above interannual and interdecadal dynamics.

4.2. Magnitudes of N_2 Fixation and Potential Impacts on Biomass Production and Nitrogen Inventory of the ETSP

Averaged over the entire water column (0–300 m), our volumetric rates ($1.19 \pm 3.81 nmol N L^{-1} d^{-1}$, $n = 103$ measurements) are in agreement with the global average of N_2 fixation rates ($1.4 \pm 4.6 nmol N L^{-1} d^{-1}$) reported

from coastal regions by Tang, Li, and Cassar (2019), Tang, Wang, et al. (2019), and other observations from the ETSP (Bonnet et al., 2013; Chang et al., 2019; Dekaezemacker et al., 2013; Fernandez et al., 2011; Knapp et al., 2016; Löscher et al., 2014; Selden et al., 2021).

When integrated through the water column (5–250 m), areal N_2 fixation rates (18.12–582.11 $\mu\text{mol N m}^{-2} \text{d}^{-1}$, Figure 1b) are within the range but on the lower end of the integrated rates (0–400 m, 2–950 $\mu\text{mol N m}^{-2} \text{d}^{-1}$) reported from the ETSP by Fernandez et al. (2011). Save for the highest areal rate (582.11 $\mu\text{mol N m}^{-2} \text{d}^{-1}$), most of our rates are lower (<200 $\mu\text{mol N m}^{-2} \text{d}^{-1}$) than the average model predictions of N_2 fixation for the region (~500 $\mu\text{mol N m}^{-2} \text{d}^{-1}$) by Deutsch et al. (2007). In line with several model results, our data confirm that predicted N_2 fixation rates may be overestimated (Moore & Doney, 2007; Wang et al., 2019), especially considering that observed N_2 fixation rates from the ETSP are comparably lower in austral winter (Chang et al., 2019).

Our sampling strategy focused on the coastal band where the highest volumetric N_2 fixation rates (up to 800 $\mu\text{mol N m}^{-2} \text{d}^{-1}$) have been measured to date (Löscher et al., 2014, 2016). Episodic sulfidic events, now commonly reported from the Peruvian OMZ and eddy events (Schlosser et al., 2018; Schunck et al., 2013), were previously associated with the high coastal N_2 fixation rates and gammaproteobacterial diazotrophic activity along 12°S (Station 19, 12° 30'S 77°W) by Löscher et al. (2014, 2016). This suggests that N_2 fixation in the ETSP may be significantly enhanced under extreme episodic sulfidic events (Löscher et al., 2014). These high N_2 fixation rates indicate that despite the patchiness, the dominating diazotrophic community in the ETSP is capable of high N_2 fixation rates comparable to those measured during *Trichodesmium* blooms in the North Atlantic, if exposed to the right environmental conditions (Capone et al., 2005; Fonseca-Batista et al., 2019; Mulholland et al., 2012). In contrast to Löscher et al. (2014), we measured eight times lower integrated N_2 fixation rates of 162.95 $\mu\text{mol m}^{-2} \text{d}^{-1}$ along the same latitude (Station 46 at 12°S, 78°W), the closest station to Station 19 of Löscher et al. (2014), a decade later but during the same season. Furthermore, it should also be noted that for a large number of N_2 fixation rates from previous studies in the HUS and reported herein, N_2 fixation rates were consistently below detection. Hence, whilst the potential for high N_2 fixation rates may exist in the northern HUS, our study demonstrates an uncertainty of whether these high N_2 fixation rates are sustained over time. Considering that previous studies have similarly reported both detectable and low to no N_2 fixation in the northern HUS, N_2 fixation rates seem widely variable and intermittent both spatially and temporally (Chang et al., 2019; Dekaezemacker et al., 2013; Löscher et al., 2014; Selden et al., 2021). Nonetheless, while N_2 fixation may occur year-round, N_2 fixation rates in the coastal waters of the northern HUS during austral summer do not seem to be substantially high, as hypothesized by Deutsch et al. (2007). These results provide further evidence to support previous conclusions that the ETSP is likely not a “hotspot” for N_2 fixation (Chang et al., 2019; Knapp et al., 2016; Selden et al., 2021; Wang et al., 2019). Nevertheless, the temporal variability of N_2 fixation needs to be considered in regional nitrogen budgets since coastal waters may have a previously underestimated contribution to new nitrogen inputs in the HUS when N_2 fixation rates are episodically enhanced.

Net ^{13}C primary production rates measured in the same incubation bottles as N_2 fixation ranged between 0.02–104.09 $\mu\text{mol C L}^{-1} \text{d}^{-1}$ with an average mean of $17.00 \pm 28.41 \mu\text{mol C L}^{-1} \text{d}^{-1}$ from the euphotic zone (Kittu, Fernández-Méndez et al., 2021; Kittu, Hopwood, et al., 2021; Kittu, Paul, et al., 2021). Assuming a Redfield ratio (C:N ~ 6.6) (Redfield, 1958), we calculated that the contribution of measured N_2 fixation to the new primary production by providing new nitrogen to the euphotic zone ranged between ~0.0 and 0.50% (average, $0.05 \pm 0.11\%$). This demonstrates that N_2 fixation was a measurable but minor source of new nitrogen to support local new primary productivity during our cruise. It is therefore evident that other N sources for example, from upwelled nitrate or regenerative nutrients (e.g., ammonium), are more important for supporting the observed high primary productivity in the region (Fernández et al., 2009; Hauschildt et al., 2021).

Nevertheless, the occurrence of N_2 fixation in the coastal waters of the northern HUS might be relevant for N cycling in the highly productive Peruvian upwelling system due to the extent to which it counterbalances bioavailable N loss. Our observations do support the Deutsch et al. (2007) hypothesis for a collocation of N_2 fixation and bioavailable N loss in the southern coastal productive waters off Peru, which may be important for feedbacks on the nitrogen inventory in the region (Landolfi et al., 2013). To assess this, we considered the distribution of N loss estimates from N_{def} calculations and secondary NO_2^- maxima measurements. Using estimates of microbial respiration and NO_3^- deficit, Codispoti and Packard (1980) established that 76% of the total N loss in the ETSP occurs from the main secondary NO_2^- maxima zone (>2 $\mu\text{mol L}^{-1}$), within a 175 km band from the coast. Based on these estimates, they demarcated a coastal area of $3.26 \times 10^{11} \text{m}^{-2}$ between 10°S and 25°S where NO_2^- concentrations

were positively correlated with denitrification rates. Our sampling area (8–16°S) covered approximately half of the total area demarcated with pronounced N loss. N₂ fixation rates between Transects 3 and 6 were associated with surface and subsurface waters featuring a calculated high N_{def} (Figure 5b, 5–25 μmol L⁻¹) and a pronounced secondary NO₂⁻ maxima in O₂ deficient coastal waters (NO₂⁻ range = 2–8 μmol L⁻¹) starting from 30 m deep (Codispoti & Packard, 1980; Kalvelage et al., 2013). Within this area, high denitrification and anammox rates of up to ~6.1 mmol N m⁻² d⁻¹ amounting to a total N loss of 12 Tg N yr⁻¹ have been reported (Karthäuser et al., 2021).

To account for the potential biogeochemical significance of N₂ fixation in the ETSP, we compared reported estimates of N loss in the ETSP (range 9–25 Tg N yr⁻¹, Kalvelage et al., 2013; Karthäuser et al., 2021) to N₂ fixation rates measured during our study. We applied a similar approach to Karthäuser et al. (2021) and Bonnet et al. (2013) by considering the same spatial extent of N₂ fixation as for N loss to extrapolate our rates and roughly estimate annual N₂ fixation inputs over the entire area of the coastal OMZ susceptible to N loss (3.26 × 10¹¹ m²). Using an integrated N₂ fixation rate of 69.46 ± 120.02 μmol N m⁻² d⁻¹ averaged from 25 stations within 175 km from the coast, total N₂ fixation potentially amounts to ~0–0.32 Tg N yr⁻¹, replenishing ~0 to 1.3% of the N lost. Based on these estimates, N₂ fixation rates from the region would need to be 10–100-fold higher to balance the N loss, therefore demonstrating the low potential for austral summer N₂ fixation rates to compensate for N loss in the coastal waters of the northern HUS off Peru. While these are only rough estimates of the potential importance of N₂ fixation in the northern HUS, we note that our estimates are on the lower end of annual estimates of N₂ fixation rates for the ETSP reported by Bonnet et al. (2013), which included rates from further offshore and toward the end of austral summer (0.16%–10%). Potential explanations for this difference could be that our samples, taken up to 300 m did not cover the extent of aphotic waters at depth (up to 2,000 m) from where N₂ fixation rates were attributed to largely contribute to total areal N₂ fixation in the ETSP (Bonnet et al., 2013). Additionally, we note that while intense denitrification and anammox are mainly restricted to the subsurface anoxic and suboxic waters within the 175 km coastal band (Kalvelage et al., 2013), N₂ fixation in the ETSP occurs over a larger spatial extent, albeit at much lower rates in the open ocean and aphotic waters beyond 300 m (Bonnet et al., 2013; Chang et al., 2019; Dekaezemacker et al., 2013; Löscher et al., 2014; Selden et al., 2021). Considering the large area of aphotic and open waters, even low but persistent N₂ fixation rates may significantly contribute to higher estimates if annually sustained. Therefore, the spatial scale and coverage of N₂ fixation over which rates are measured and extrapolated are therefore important to consider for these comparisons. Hence, our estimates from only the coastal region within 300 m depth may be underestimated, especially considering the high variability observed in N₂ fixation rates within this study and potential seasonal variability yet to be thoroughly investigated. To better understand the relationships between these two processes, we recommend that both measurements of N₂ fixation and N loss processes should be taken from the same samples in parallel across different seasons and on a broader spatial scale in the ETSP than considered herein.

In general, our results highlight that while the spatial coupling of N₂ fixation and N loss is evident in coastal waters of the ETSP associated with an intense OMZ (Dekaezemacker et al., 2013; Löscher et al., 2014), this doesn't necessarily suggest that N₂ fixation counterbalances the high N loss reported from the region. The collocation of these two processes, as shown in this study, supports the hypothesis that self-reinforcing positive feedbacks on the N cycle are likely to occur at the local scale (Landolfi et al., 2013). Considering the stoichiometric imbalance in N₂ fixation and N loss (Landolfi et al., 2013), the significance of N₂ fixation in the ETSP may be more related to the feedback that ensues in the N inventory rather than to its minor direct role in nitrogen supply for primary productivity. At least for summer conditions in this study, the presence of N₂ fixation in proximity to low oxygen N deficient waters along the coast could enhance the N deficit, thereby creating a self-sustaining cycle between N loss and N₂ fixation that results in net N loss locally. Hence, on short (e.g., annual) time scales and considering temporal variability in N₂ fixation rates, our results suggest that the hypothesized positive feedback on the N inventory of the northern HUS (Landolfi et al., 2013) could be strengthened by enhanced N₂ fixation in the coastal waters where both phytoplankton productivity and N loss are high. If the hypothesis of a vicious cycle holds, collocation of N loss and N₂ fixation in the coastal OMZ of the northern HUS could trigger regional changes in the N inventory (Landolfi et al., 2013). These stoichiometry-driven changes in the size of the local N inventory may lead to bottom-up-regulated perturbations in food web dynamics and the efficiency of the biological pump at a local scale (Falkowski, 1997). Over longer time scales, however, the N loss in the northern HUS has been hypothesized to be counterbalanced by basin-wide N inputs through high N₂ fixation rates observed in the Western Tropical Pacific (Bonnet et al., 2017; Wang et al., 2019). However, for a local replenishment, it is

still unclear whether such a large increase in annual N_2 fixation rates, 10–100 fold to be proportional to local N loss estimates, is regionally plausible in the ETSP.

5. Conclusion

This study provides the highest resolution of the spatial distribution of N_2 fixation reported so far from the northern HUS, with a stronger focus on coastal waters compared to previous studies. Our data revealed notable latitudinal differences in N_2 fixation in the northern HUS coinciding with a similar latitudinal pattern in N loss. N_2 fixation was below detection in the northern transects between 8 and 10°S and increased from the central to southern transects toward the region of intensified N loss and higher primary productivity (12°S–16°S). This indicates that N_2 fixation in the northern HUS may be mostly confined to the southern part of coastal waters above and within the region of intense N loss. This latitudinal pattern is likely a result of a complex interplay of multiple environmental factors, including organic matter availability, and potential factors that regulate it, such as the availability of trace metals (Fe). These factors may have direct and indirect effects on the regional distribution of N_2 fixation in coastal waters of the northern HUS off Peru. Despite the observed negligible contribution of diazotrophy to supporting new primary productivity, the collocation of low N_2 fixation and high bioavailable N loss (nitrate and ammonia loss via denitrification and anammox) close to the coast provide evidence that there is potential for a local self-sustaining feedback along the coast that could potentially lead to a runaway loss of N as previously hypothesized. Hence, we postulate that on short timescales, this positive feedback could be strengthened via future changes in deoxygenation, phytoplankton organic matter production, and trace metal biogeochemistry, especially in relation to sporadic occurrences of sulfidic events. However, further studies are required to quantify and determine the strength, and biogeochemical and ecological implications of this positive feedback for the coastal system as N_2 fixation rates would need to be 10–100 fold higher than currently measured rates to match the rates of N loss from the same region. Additionally, temporal shifts in N_2 fixation rates associated with seasonality need to be accounted for, which is challenging due to the current patchy distribution of observed N_2 fixation rates.

Data Availability Statement

The data sets are available on PANGAEA as follows:

- N_2 fixation rates (Kittu, Paul, et al., 2021).
- Water column biogeochemistry (Kittu, Fernández-Méndez et al., 2021).
- TdFe concentrations (Kittu, Hopwood, et al., 2021).

Acknowledgments

This research was supported by the German Federal Ministry of Education and Research (BMBF) through the cooperative research projects Humboldt Tipping (01LC1823B) and CUSCO (“Coastal Upwelling System in a Changing Ocean,” FKZ03F0). The authors are grateful to the captains, crew members, and scientists onboard the MSM80 cruise of the German R/V Maria S Merian for their support and cooperation at sea. We especially thank Joaquin Ortiz, Michael Meyerhöfer, and Rainer Kiko for assisting with onboard sampling and Kastriot Qelaj for nutrient sampling and analysis. We also thank Kerstin Nachtigall for assistance with sample analysis for mass spectrometry and Silvia Georgieva for providing help with processing and data analysis. Thanks to Carolin Löscher for her helpful comments on earlier versions of the manuscript. Open Access funding enabled and organized by Projekt DEAL.

References

- Bevington, P., & Robinson, D. K. (2002). *Data reduction and error analysis for the physical sciences* (Revised edition). McGraw Hill Book Co.
- Blain, S., Bonnet, S., & Guieu, C. (2008). Dissolved iron distribution in the tropical and sub-tropical South Eastern Pacific. *Biogeochemistry*, 5(1), 269–280. <https://doi.org/10.5194/bg-5-269-2008>
- Bombar, D., Paerl, R. W., & Riemann, L. (2016). Marine non-cyanobacterial diazotrophs: Moving beyond molecular detection. *Trends in Microbiology*, 24(11), 916–927. <https://doi.org/10.1016/j.tim.2016.07.002>
- Bonnet, S., Cuffin, M., Berthelot, H., & Moutin, T. (2017). Hot spot of N_2 fixation in the western tropical South Pacific pleads for a spatial decoupling between N_2 fixation and denitrification. *Proceedings of the National Academy of Sciences of the United States of America*, 114(14), E2800–E2801. <https://doi.org/10.1073/pnas.1619514114>
- Bonnet, S., Dekazemacker, J., Turk-Kubo, K. A., Moutin, T., Hamersley, R. M., Grosso, O., et al. (2013). Aphotic N_2 fixation in the eastern tropical South Pacific Ocean. *PLoS One*, 8(12), e81265. <https://doi.org/10.1371/journal.pone.0081265>
- Bonnet, S., Guieu, C., Bruyant, F., Prášil, O., Van Wambeke, F., Raimbault, P., et al. (2008). Nutrient limitation of primary productivity in the Southeast Pacific (BIOCOPE cruise). *Biogeochemistry*, 5(1), 215–225. <https://doi.org/10.5194/bg-5-215-2008>
- Browning, T. J., Rapp, I., Schlosser, C., Gledhill, M., Achterberg, E. P., Bracher, A., & Moigne, F. A. C. L. (2018). Influence of iron, cobalt, and vitamin B₁₂ supply on phytoplankton growth in the tropical East Pacific during the 2015 El Niño. *Geophysical Research Letters*, 45(12), 6150–6159. <https://doi.org/10.1029/2018GL077972>
- Bruland, K. W., Rue, E. L., Smith, G. J., & DiTullio, G. R. (2005). Iron, macronutrients and diatom blooms in the Peru upwelling regime: Brown and blue waters of Peru. *Marine Chemistry*, 93(2), 81–103. <https://doi.org/10.1016/j.marchem.2004.06.011>
- Capone, D. G., Burns, J. A., Montoya, J. P., Subramaniam, A., Mahaffey, C., Gunderson, T., et al. (2005). Nitrogen fixation by *Trichodesmium* spp.: An important source of new nitrogen to the tropical and subtropical North Atlantic Ocean. *Global Biogeochemical Cycles*, 19(2), GB2024. <https://doi.org/10.1029/2004GB002331>
- Chakraborty, S., Andersen, K. H., Visser, A. W., Inomura, K., Follows, M. J., & Riemann, L. (2021). Quantifying nitrogen fixation by heterotrophic bacteria in sinking marine particles. *Nature Communications*, 12(1), 4085. <https://doi.org/10.1038/s41467-021-23875-6>
- Chang, B. X., Devol, A. H., & Emerson, S. R. (2010). Denitrification and the nitrogen gas excess in the eastern tropical South Pacific oxygen deficient zone. *Deep Sea Research Part I: Oceanographic Research Papers*, 57(9), 1092–1101. <https://doi.org/10.1016/j.dsr.2010.05.009>

- Chang, B. X., Jayakumar, A., Widner, B., Bernhardt, P., Mordy, C. W., Mulholland, M. R., & Ward, B. B. (2019). Low rates of dinitrogen fixation in the eastern tropical South Pacific. *Limnology & Oceanography*, *64*(5), 1913–1923. <https://doi.org/10.1002/lno.11159>
- Cheung, S., Zehr, J. P., Xia, X., Tsurumoto, C., Endo, H., Nakaoka, S., et al. (2021). Gamma4: A genetically versatile gammaproteobacterial nifH phylotype that is widely distributed in the North Pacific ocean. *Environmental Microbiology*, *23*(8), 4246–4259. <https://doi.org/10.1111/1462-2920.15604>
- Chever, F., Rouxel, O. J., Croot, P. L., Ponzevera, E., Wuttig, K., & Auro, M. (2015). Total dissolvable and dissolved iron isotopes in the water column of the Peru upwelling regime. *Geochimica et Cosmochimica Acta*, *162*, 66–82. <https://doi.org/10.1016/j.gca.2015.04.031>
- Hiroshi Akima [aut, cph] (Fortran code (TOMS 760, 761, 697 and 433)), Albrecht Gebhardt [aut, cre, cph] (R port (interp*, bicubic* functions), bilinear code), Thomas Petzold [ctb, cph] (aspline function), Martin Maechler [ctb, cph] (interp2xyz function + enhancements), YYY Association for Computing Machinery, Inc. [cph] (covers code from TOMS 760, 761, 697 and 433) (2021). akima: Interpolation of irregularly and regularly spaced data (version 0.6-2.3). Retrieved from <https://CRAN.R-project.org/package=akima>
- Codispoti, L. A., Brandes, J. A., Christensen, J. P., Devol, A. H., Naqvi, S. W. A., Paerl, H. W., & Yoshinari, T. (2001). The oceanic fixed nitrogen and nitrous oxide budgets: Moving targets as we enter the Anthropocene? *Scientia Marina*, *65*(S2), 85–105. <https://doi.org/10.3989/scimar.2001.65s285>
- Codispoti, L. A., & Packard, T. T. (1980). Denitrification rates in the eastern tropical South Pacific. (Vol. 38).
- Dekazemacker, J., Bonnet, S., Grosso, O., Moutin, T., Bressac, M., & Capone, D. G. (2013). Evidence of active dinitrogen fixation in surface waters of the eastern tropical South Pacific during El Niño and La Niña events and evaluation of its potential nutrient controls. *Global Biogeochemical Cycles*, *27*(3), 768–779. <https://doi.org/10.1002/gbc.20063>
- Deutsch, C., Sarmiento, J. L., Sigman, D. M., Gruber, N., & Dunne, J. P. (2007). Spatial coupling of nitrogen inputs and losses in the ocean. *Nature*, *445*(7124), 163–167. <https://doi.org/10.1038/nature05392>
- DeVries, T., Deutsch, C., Primeau, F., Chang, B., & Devol, A. (2012). Global rates of water-column denitrification derived from nitrogen gas measurements. *Nature Geoscience*, *5*(8), 547–550. <https://doi.org/10.1038/ngeo1515>
- Dutkiewicz, S., Ward, B. A., Monteiro, F., & Follows, M. J. (2012). Interconnection of nitrogen fixers and iron in the Pacific Ocean: Theory and numerical simulations. *Global Biogeochemical Cycles*, *26*(1), GB1012. <https://doi.org/10.1029/2011GB004039>
- Dyrman, S. T., & Haley, S. T. (2006). Phosphorus scavenging in the unicellular marine diazotroph *Crocospaera watsonii*. *Applied and Environmental Microbiology*, *72*(2), 1452–1458. <https://doi.org/10.1128/AEM.72.2.1452-1458.2006>
- Falkowski, P. G. (1997). Evolution of the nitrogen cycle and its influence on the biological sequestration of CO₂ in the ocean. *Nature*, *387*(6630), 272–275. <https://doi.org/10.1038/387272a0>
- Farnelid, H., & Riemann, L. (2008). Heterotrophic N₂-fixing bacteria: Overlooked in the marine nitrogen cycle? In *Nitrogen fixation research progress* (pp. 409–423).
- Fernández, C., Fariás, L., & Alcaman, M. E. (2009). Primary production and nitrogen regeneration processes in surface waters of the Peruvian upwelling system. *Progress in Oceanography*, *83*(1), 159–168. <https://doi.org/10.1016/j.poccean.2009.07.010>
- Fernandez, C., Fariás, L., & Ulloa, O. (2011). Nitrogen fixation in denitrified marine waters. *PLoS One*, *6*(6), e20539. <https://doi.org/10.1371/journal.pone.0020539>
- Fernandez, C., González, M. L., Muñoz, C., Molina, V., & Fariás, L. (2015). Temporal and spatial variability of biological nitrogen fixation off the upwelling system of central Chile (35–38.5°S). *Journal of Geophysical Research: Oceans*, *120*(5), 3330–3349. <https://doi.org/10.1002/2014JC010410>
- Fonseca-Batista, D., Li, X., Riou, V., Michotey, V., Deman, F., Fripiat, F., et al. (2019). Evidence of high N₂ fixation rates in the temperate north-east Atlantic. *Biogeosciences*, *16*(5), 999–1017. <https://doi.org/10.5194/bg-16-999-2019>
- Gradoville, M. R., Deniz, B., Crump Byron, C., Letelier Ricardo, M., Zehr Jonathan, P., & White Angelique, E. (2017). Diversity and activity of nitrogen-fixing communities across ocean basins. *Limnology & Oceanography*, *62*(5), 1895–1909. <https://doi.org/10.1002/lno.10542>
- Großkopf, T., Mohr, W., Baustian, T., Schunck, H., Gill, D., Kuypers, M. M. M., et al. (2012). Doubling of marine dinitrogen-fixation rates based on direct measurements. *Nature*, *488*(7411), 361–364. <https://doi.org/10.1038/nature11338>
- Gruber, N. (2004). The dynamics of the marine nitrogen cycle and its influence on atmospheric CO₂ variations. In M. Follows & T. Oguz (Eds.), *The Ocean carbon cycle and climate* (pp. 97–148). Springer Netherlands. https://doi.org/10.1007/978-1-4020-2087-2_4
- Gruber, N., & Galloway, J. N. (2008). An Earth-system perspective of the global nitrogen cycle. *Nature*, *451*(7176), 293–296. <https://doi.org/10.1038/nature06592>
- Hammersley, M. R., Lavik, G., Woebken, D., Rattray, J. E., Lam, P., Hopmans, E. C., et al. (2007). Anaerobic ammonium oxidation in the Peruvian oxygen minimum zone. *Limnology & Oceanography*, *52*(3), 923–933. <https://doi.org/10.4319/lno.2007.52.3.0923>
- Hansen, H. P., & Koroleff, F. (1999). Determination of nutrients. In *Methods of seawater analysis* (pp. 159–228). John Wiley & Sons, Ltd. <https://doi.org/10.1002/9783527613984.ch10>
- Hauschildt, J., Thomsen, S., Echevin, V., Oschlies, A., José, Y. S., Krahnmann, G., et al. (2021). The fate of upwelled nitrate off Peru shaped by sub-mesoscale filaments and fronts. *Biogeosciences*, *18*(12), 3605–3629. <https://doi.org/10.5194/bg-18-3605-2021>
- Holmes, R. M., Aminot, A., Kérouel, R., Hooker, B. A., & Peterson, B. J. (2011). A simple and precise method for measuring ammonium in marine and freshwater ecosystems. *Canadian Journal of Fisheries and Aquatic Sciences*, *56*(10), 1801–1808. <https://doi.org/10.1139/f99-128>
- Hopwood, M. J., Meyer, J., Achterberg, E. P., Gledhill, M., Mutzberg, A., & Nehir, M. (2021). Trace metal data from water samples during METEOR cruise M135 [Dataset]. PANGAEA. <https://doi.org/10.1594/PANGAEA.928117>
- Hutchins, D. A., Hare, C. E., Weaver, R. S., Zhang, Y., Firme, G. F., Ditullio, G. R., et al. (2002). Phytoplankton iron limitation in the Humboldt current and Peru upwelling. *Limnology & Oceanography*, *47*(4), 997–1011. <https://doi.org/10.4319/lno.2002.47.4.0997>
- Inomura, K., Bragg, J., & Follows, M. J. (2017). A quantitative analysis of the direct and indirect costs of nitrogen fixation: A model based on azotobacter vinelandii. *The ISME Journal*, *11*(1), 166–175. <https://doi.org/10.1038/ismej.2016.97>
- Jayakumar, A., & Ward, B. B. (2020). Diversity and distribution of nitrogen fixation genes in the oxygen minimum zones of the world oceans. *Biogeosciences*, 1–28. <https://doi.org/10.5194/bg-17-5953-2020>
- Kalvelage, T., Lavik, G., Lam, P., Contreras, S., Arteaga, L., Löscher, C. R., et al. (2013). Nitrogen cycling driven by organic matter export in the South Pacific oxygen minimum zone. *Nature Geoscience*, *6*(3), 228–234. <https://doi.org/10.1038/ngeo1739>
- Karl, D. M., Church, M. J., Dore, J. E., Letelier, R. M., & Mahaffey, C. (2012). Predictable and efficient carbon sequestration in the North Pacific Ocean supported by symbiotic nitrogen fixation. *Proceedings of the National Academy of Sciences of the United States of America*, *109*(6), 1842–1849. <https://doi.org/10.1073/pnas.1120312109>
- Karstensen, J., Stramma, L., & Visbeck, M. (2008). Oxygen minimum zones in the eastern tropical Atlantic and Pacific Oceans. *Progress in Oceanography*, *77*(4), 331–350. <https://doi.org/10.1016/j.poccean.2007.05.009>
- Karthäuser, C., Ahmerkamp, S., Marchant, H. K., Bristow, L. A., Hauss, H., Iversen, M. H., et al. (2021). Small sinking particles control anammox rates in the Peruvian oxygen minimum zone. *Nature Communications*, *12*(1), 3235. <https://doi.org/10.1038/s41467-021-23340-4>

- Kittu, L., Fernández-Méndez, M., Paul, A. J., Kiko, R., & Riebesell, U. (2021). Dissolved inorganic and organic nutrients from water column samples during RV Maria S. Merian cruise MSM80 off the northern Humboldt Upwelling System [Dataset]. PANGAEA. <https://doi.org/10.1594/PANGAEA.939667>
- Kittu, L., Hopwood, M. J., Paul, A. J., Fernández-Méndez, M., Achterberg, E. P., & Riebesell, U. (2021). Trace metal data from water column samples during RV Maria S. Merian cruise MSM80 off the northern Humboldt Upwelling System [Dataset]. PANGAEA. <https://doi.org/10.1594/PANGAEA.939670>
- Kittu, L., Paul, A. J., Fernández-Méndez, M., & Riebesell, U. (2021). Nitrogen and carbon fixation rates and organic matter concentrations from water column samples during RV Maria S. Merian cruise MSM80 off the northern Humboldt Upwelling System [Dataset]. PANGAEA. <https://doi.org/10.1594/PANGAEA.939726>
- Klawonn, I., Bonaglia, S., Brüchert, V., & Ploug, H. (2015). Aerobic and anaerobic nitrogen transformation processes in N_2 -fixing cyanobacterial aggregates. *The ISME Journal*, 9(6), 1456–1466. <https://doi.org/10.1038/ismej.2014.232>
- Knapp, A. N., Casciotti, K. L., Berelson, W. M., Prokopenko, M. G., & Capone, D. G. (2016). Low rates of nitrogen fixation in eastern tropical South Pacific surface waters. *Proceedings of the National Academy of Sciences of the United States of America*, 113(16), 4398–4403. <https://doi.org/10.1073/pnas.1515641113>
- Kustka, A. B., Sañudo-Wilhelmy, S. A., Carpenter, E. J., Capone, D., Burns, J., & Sunda, W. G. (2003). Iron requirements for dinitrogen- and ammonium-supported growth in cultures of *Trichodesmium* (IMS 101): Comparison with nitrogen fixation rates and iron: Carbon ratios of field populations. *Limnology & Oceanography*, 49(4), 1869–1884. <https://doi.org/10.4319/lo.2003.48.5.1869>
- Lam, P., Lavik, G., Jensen, M. M., van de Vossenber, J., Schmid, M., Woebken, D., et al. (2009). Revising the nitrogen cycle in the Peruvian oxygen minimum zone. *Proceedings of the National Academy of Sciences of the United States of America*, 106(12), 4752–4757. <https://doi.org/10.1073/pnas.0812444106>
- Landolfi, A., Dietze, H., Koeve, W., & Oschlies, A. (2013). Overlooked runaway feedback in the marine nitrogen cycle: The vicious cycle. *Biogeosciences*, 10(3), 1351–1363. <https://doi.org/10.5194/bg-10-1351-2013>
- Löscher, C. R., Bourbonnais, A., Dekaezemacker, J., Charoenpong, C. N., Altabet, M. A., Bange, H. W., et al. (2016). N_2 fixation in eddies of the eastern tropical South Pacific Ocean. *Biogeosciences*, 13(10), 2889–2899. <https://doi.org/10.5194/bg-13-2889-2016>
- Löscher, C. R., Großkopf, T., Desai, F. D., Gill, D., Schunck, H., Croot, P. L., et al. (2014). Facets of diazotrophy in the oxygen minimum zone waters off Peru. *The ISME Journal*, 8(11), 2180–2192. <https://doi.org/10.1038/ismej.2014.71>
- Luo, Y.-W., Lima, I. D., Karl, D. M., Deutsch, C. A., & Doney, S. C. (2014). Data-based assessment of environmental controls on global marine nitrogen fixation. *Biogeosciences*, 11(3), 691–708. <https://doi.org/10.5194/bg-11-691-2014>
- Messié, M., & Chavez, F. P. (2015). Seasonal regulation of primary production in eastern boundary upwelling systems. *Progress in Oceanography*, 134, 1–18. <https://doi.org/10.1016/j.pocean.2014.10.011>
- Meyer, J., Löscher, C. R., Lavik, G., & Riebesell, U. (2017). Mechanisms of P^* reduction in the eastern Tropical South Pacific. *Frontiers in Marine Science*, 4. <https://doi.org/10.3389/fmars.2017.00001>
- Meyer, J., Löscher, C. R., Neulinger, S. C., Reichel, A. F., Loginova, A., Borchard, C., et al. (2016). Changing nutrient stoichiometry affects phytoplankton production, DOP accumulation, and dinitrogen fixation—A mesocosm experiment in the eastern tropical North Atlantic. *Biogeosciences*, 13(3), 781–794. <https://doi.org/10.5194/bg-13-781-2016>
- Mohr, W., Großkopf, T., Wallace, D. W. R., & LaRoche, J. (2010). Methodological underestimation of oceanic nitrogen fixation rates. *PLoS One*, 5(9), e12583. <https://doi.org/10.1371/journal.pone.0012583>
- Montoya, J. P., Voss, M., Kahler, P., & Capone, D. G. (1996). A simple, high-precision, high sensitivity tracer assay for N_2 fixation. *Applied and Environmental Microbiology*, 62(3), 986–993. <https://doi.org/10.1128/aem.62.3.986-993.1996>
- Moore, C. M. (2016). Diagnosing oceanic nutrient deficiency. *Philosophical Transactions of the Royal Society A: Mathematical, Physical & Engineering Sciences*, 374(2081), 20150290. <https://doi.org/10.1098/rsta.2015.0290>
- Moore, C. M., Mills, M. M., Arrigo, K. R., Berman-Frank, I., Bopp, L., Boyd, P. W., et al. (2013). Processes and patterns of oceanic nutrient limitation. *Nature Geoscience*, 6(9), 701–710. <https://doi.org/10.1038/ngeo1765>
- Moore, J. K., & Doney, S. C. (2007). Iron availability limits the ocean nitrogen inventory stabilizing feedbacks between marine denitrification and nitrogen fixation. *Global Biogeochemical Cycles*, 21(2), GB2001. <https://doi.org/10.1029/2006GB002762>
- Morris, A. W., & Riley, J. P. (1963). The determination of nitrate in sea water. *Analytica Chimica Acta*, 29, 272–279. [https://doi.org/10.1016/S0003-2670\(00\)88614-6](https://doi.org/10.1016/S0003-2670(00)88614-6)
- Mulholland, M. R., Bernhardt, P. W., Blanco-Garcia, J. L., Mannino, A., Hyde, K., Mondragon, E., et al. (2012). Rates of dinitrogen fixation and the abundance of diazotrophs in North American coastal waters between Cape Hatteras and Georges Bank. *Limnology & Oceanography*, 57(4), 1067–1083. <https://doi.org/10.4319/lo.2012.57.4.1067>
- Murphy, J., & Riley, J. P. (1962). A modified single solution method for the determination of phosphate in natural waters. *Analytica Chimica Acta*, 27, 31–36. [https://doi.org/10.1016/S0003-2670\(00\)88444-5](https://doi.org/10.1016/S0003-2670(00)88444-5)
- NASA/JPL. (2020). MODIS aqua level 3 SST thermal IR annual 4km daytime V2019.0 [Dataset]. NASA Physical Oceanography DAAC. <https://doi.org/10.5067/MODSA-AN4D9>
- NASA Ocean Biology Processing Group. (2017). MODIS-aqua level 3 mapped chlorophyll data version R2018.0 [Dataset]. NASA Ocean Biology DAAC. <https://doi.org/10.5067/AQUA/MODIS/L3M/CHL/2018>
- Noffke, A., Hensen, C., Sommer, S., Scholz, F., Bohlen, L., Mosch, T., et al. (2012). Benthic iron and phosphorus fluxes across the Peruvian oxygen minimum zone. *Limnology & Oceanography*, 57(3), 851–867. <https://doi.org/10.4319/lo.2012.57.3.0851>
- Parekh, P., Follows, M. J., & Boyle, E. A. (2005). Decoupling of iron and phosphate in the global ocean. *Global Biogeochemical Cycles*, 19(2), GB2020. <https://doi.org/10.1029/2004GB002280>
- Paulmier, A., Kriest, I., & Oschlies, A. (2009). Stoichiometries of remineralisation and denitrification in global biogeochemical ocean models. *Biogeosciences*, 6(5), 923–935. <https://doi.org/10.5194/bg-6-923-2009>
- Rapp, I., Schlosser, C., Browning, T. J., Wolf, F., Moigne, F. A. C. L., Gledhill, M., & Achterberg, E. P. (2020). El Niño-driven oxygenation impacts Peruvian shelf iron supply to the South Pacific ocean. *Geophysical Research Letters*, 47(7), e2019GL086631. <https://doi.org/10.1029/2019GL086631>
- Rapp, I., Schlosser, C., Rusiecka, D., Gledhill, M., & Achterberg, E. P. (2017). Automated preconcentration of Fe, Zn, Cu, Ni, Cd, Pb, Co, and Mn in seawater with analysis using high-resolution sector field inductively-coupled plasma mass spectrometry. *Analytica Chimica Acta*, 976, 1–13. <https://doi.org/10.1016/j.aca.2017.05.008>
- Redfield, A. C. (1958). The biological control of chemical factors in the environment. *American Scientist*, 46(3), 205–221.
- Riemann, L., Rahav, E., Passow, U., Hans-Peter Grossart, Dirk de Beer, Isabell Klawonn, et al. (2022). Planktonic aggregates as hotspots for heterotrophic diazotrophy: The plot thickens. *Frontiers in Microbiology*. <https://doi.org/10.3389/fmicb.2022.875050>

- Schlosser, C., Streu, P., Frank, M., Lavik, G., Croot, P. L., Dengler, M., & Achterberg, E. P. (2018). H₂S events in the Peruvian oxygen minimum zone facilitate enhanced dissolved Fe concentrations. *Scientific Reports*, 8(1), 12642. <https://doi.org/10.1038/s41598-018-30580-w>
- Schunck, H., Lavik, G., Desai, D. K., Großkopf, T., Kalvelage, T., Löscher, C. R., et al. (2013). Giant hydrogen sulfide plume in the oxygen minimum zone off Peru supports chemolithoautotrophy. *PLoS One*, 8(8), e68661. <https://doi.org/10.1371/journal.pone.0068661>
- Selden, C. R., Mulholland, M. R., Widner, B., Bernhardt, P., & Jayakumar, A. (2021). Toward resolving disparate accounts of the extent and magnitude of nitrogen fixation in the Eastern Tropical South Pacific oxygen deficient zone. *Limnology & Oceanography*, 66(5), 1950–1960. <https://doi.org/10.1002/lno.11735>
- Shiozaki, T., Kodama, T., & Furuya, K. (2014). Large-scale impact of the island mass effect through nitrogen fixation in the western South Pacific Ocean. *Geophysical Research Letters*, 41(8), 2907–2913. <https://doi.org/10.1002/2014GL059835>
- Somes, C. J., & Oschlies, A. (2015). On the influence of “non-Redfield” dissolved organic nutrient dynamics on the spatial distribution of N₂ fixation and the size of the marine fixed nitrogen inventory. *Global Biogeochemical Cycles*, 29(7), 973–993. <https://doi.org/10.1002/2014GB005050>
- Tang, W., Li, Z., & Cassar, N. (2019). Machine learning estimates of global marine nitrogen fixation. *Journal of Geophysical Research: Biogeosciences*, 124(3), 717–730. <https://doi.org/10.1029/2018JG004828>
- Tang, W., Wang, S., Fonseca-Batista, D., Dehairs, F., Gifford, S., Gonzalez, A. G., et al. (2019). Revisiting the distribution of oceanic N₂ fixation and estimating diazotrophic contribution to marine production. *Nature Communications*, 10(1), 831. <https://doi.org/10.1038/s41467-019-08640-0>
- Turk-Kubo, K. A., Gradoville, M. R., Cheung, S., Cornejo-Castillo, F. M., Harding, K. J., Morando, M., et al. (2022). Non-cyanobacterial diazotrophs: Global diversity, distribution, ecophysiology, and activity in marine waters. *FEMS Microbiology Reviews*. <https://doi.org/10.1093/femsre/fuac046>
- Turk-Kubo, K. A., Karamchandani, M., Capone, D. G., & Zehr, J. P. (2014). The paradox of marine heterotrophic nitrogen fixation: Abundances of heterotrophic diazotrophs do not account for nitrogen fixation rates in the eastern Tropical South Pacific. *Environmental Microbiology*, 16(10), 3095–3114. <https://doi.org/10.1111/1462-2920.12346>
- Wang, W.-L., Moore, J. K., Martiny, A. C., & Primeau, F. W. (2019). Convergent estimates of marine nitrogen fixation. *Nature*, 566(7743), 205–211. <https://doi.org/10.1038/s41586-019-0911-2>
- Ward, B. A., Dutkiewicz, S., Moore, C. M., & Follows, M. J. (2013). Iron, phosphorus, and nitrogen supply ratios define the biogeography of nitrogen fixation. *Limnology & Oceanography*, 58(6), 2059–2075. <https://doi.org/10.4319/lo.2013.58.6.2059>
- Weiss, R. F. (1970). The solubility of nitrogen, oxygen, and argon in water and seawater. *Deep-Sea Research and Oceanographic Abstracts*, 17(4), 721–735. [https://doi.org/10.1016/0011-7471\(70\)90037-9](https://doi.org/10.1016/0011-7471(70)90037-9)
- White, A. E., Granger, J., Selden, C., Gradoville, M. R., Potts, L., Bourbonnais, A., et al. (2020). A critical review of the ¹⁵N₂ tracer method to measure diazotrophic production in pelagic ecosystems. *Limnology and Oceanography: Methods*, 18(4), 129–147. <https://doi.org/10.1002/lom3.10353>
- Yang, S., Gruber, N., Long, M. C., & Vogt, M. (2017). ENSO-driven variability of denitrification and sub-oxia in the eastern tropical Pacific ocean. *Global Biogeochemical Cycles*, 31(10), 1470–1487. <https://doi.org/10.1002/2016GB005596>